Nanoprecipitation as a simple and straightforward process to create complex polymeric colloidal morphologies

Xibo Yan, Julien Bernard, François Ganachaud

Nanoprecipitation as a simple and straightforward process to create complex polymeric colloidal morphologies

Xibo Yan,*[,1] Julien Bernard,[2] and François Ganachaud[2]

[1] School of Chemical Engineering and Technology, Tianjin University, Tianjin 300072, China.

[2] Université de Lyon, Lyon, F-69003, France ; INSA-Lyon, IMP, Villeurbanne, F-69621, France; CNRS, UMR 5223, Ingénierie des Matériaux Polymères, Villeurbanne, F-69621, France.

*Corresponding author: Email: xiboyan@tju.edu.cn (X.Y.)

Abstract

Polymeric nanoparticles are deemed as important functional nanomaterials within a wide range of applications from therapeutics to energy. Advances in nanotechnology have enabled the engineering of multifunctional polymeric nanoparticles with a variety of shapes and inner morphologies. Thanks to a simple procedure, nanoprecipitation has especially become one of the most common approaches to construct polymeric nanoparticles with precise control of nanostructure. The present review highlights the great capability of nanoprecipitation technique in controlling the fabrication of various polymeric nanostructures of interest. In particular, we show here the nanoprecipitation of either block copolymers or mixtures of homopolymers. After nanoprecipitation in single colloidal components, one can generate equilibrium (typically onion-like) or non-equilibrium (stacked lamellae, porous cores) morphologies, depending whether the system "freezes" while passing the glass transition or crystallization point of starting

materials. We also show that core-shell morphologies, either all polymeric or oil/polymer states, are attainable by this one-pot process. A final discussion proposes new directions to enlarge the scope and possible achievements of the process.

Keywords: nanoprecipitation; ouzo effect; polymeric nanoparticles; self-assembly; colloidal morphology

Table of Content

1. Introduction **5**

2. Mono-component PNPs **9**

2.1 Porous nanoparticles 9
2.2 Complex internally structured nanoparticles 11

3. Multi-component PNPs **16**

3.1 Multi-faceted nanoparticles 16
3.2 Core/Shell nanoparticles and nanocapsules 21
3.2.1 Solid-core nanoparticles 21
3.2.2 Oil-filled nanocapsules 23

4. Conclusions and Future outlook **26**

References **29**

Abbreviations

AIE	Aggregation-Induced-Emission
DMF	dimethylformamide
DMSO	dimethyl sulfoxide
MD	molecular dynamic (simulation)
MW	molecular weight
NC	Nanocapsule
NMR	nuclear magnetic resonance
NP	Nanoparticle
PB	poly(butadiene)
PCBM	[6,6]-phenyl-C_{61}-butyric acid methyl ester
PCL	poly(ε-caprolactone)
PEG	polyethylene glycol
PEMM	poly(N-[2-(α-D-mannopyranosyl-oxy)ethyl] methacrylamide)
PGA	poly(glycolic acid)
P3HT	poly(3-hexylthiophene)
PFNEMA	poly(2-[(perfluorononenyl)oxy]ethyl methacrylate)
PFS	pentafluorostyrene
PHMM	poly(N-[7-(α-D-mannopyranosyloxy) heptyl] methacrylamide)
PHPMA	poly(N-(2-hydroxypropyl) methacrylamide)
PI	polyisoprene
PIB	polyisobutene
PLA	poly(lactic acid)
PLGA	poly(lactide-*co*-glycolide)
PMMA	poly(methyl methacrylate)
PS	Polystyrene
PtBA	poly(*tert*-butylacrylate)
P2VP	poly(2-vinylpyridine)
PVA	polyvinyl alcohol

PVCH	poly(vinylcyclohexane)
SEM	scanning electron microscopy
SFME	Surfactant-Free MicroEmulsion
SORP	Self-ORganized Precipitation
STEM	scanning transmission electron microscopy
TEM	transmission electron microscopy
THF	Tetrahydrofuran
VBA	4-vinylbenzyl azide
VBC	4-vinylbenzyl chloride

1. Introduction

Polymeric nanoparticles (PNPs) are soft materials with high variability in structures, compositions, properties and functions. They are playing a significant role in various applications, such as drug delivery,[1,2] bioimaging,[3] catalysis,[4] sensing,[5] construction,[6] energy and fuel cells.[7,8] With the tremendous advances in the development of PNPs over the last decades, nanostructuration has been recognized as one of the most critical parameters to affect the performance of PNPs. Distinguishing features of various nanostructures endow PNPs with great potential for applications. For instance, core/shell NPs displaying a functional polymer membrane can protect a cargo and release it in a controlled manner.[9] Janus NPs, consisting of asymmetrical polymer domains, combine drastically different functions and properties within the same single nano-object.[10] Besides, control of surface area, porosity and connectivity within the pores would theoretically allow applying NPs in gas storage, pollutant separation, catalysis, and sensing.[11] Hence, significant efforts have been made and are still devoted to design and develop PNPs with ordered nanostructures.[12-15]

Among all the methods reported for polymeric NPs preparation, nanoprecipitation (also called “Ouzo effect”, named after the Greek beverage [16,17]) is a straightforward and low energy cost technique allowing to robustly construct NPs with on-demand properties and functions. Neither high shear force techniques (e.g. ultrasonication) nor surfactants are necessary to carry out the emulsification. Also, the principle of nanoprecipitation is compatible with either hydrophobic or hydrophilic solutes for NPs generation. This spontaneous emulsification process is triggered by solvent-shifting without precursor emulsion.[18,19] The only requirement is that the solvent and the

non-solvent of the polymer remain fully miscible in all proportions. In a typical process, a solute (e.g. for instance a hydrophobic polymer) is dissolved in a solvent (e.g. ethanol, tetrahydrofuran or THF, acetone…). Upon mixing with water, the medium becomes a non-solvent for the solute, which triggers its supersaturation and phase separation from the solution, finally leading to the formation of nanoparticles in a controllable and reproducible manner. The dimensions of NPs are tunable from several tens of nanometers to submicron size.[18,20] The homogeneous dispersions prepared by nanoprecipitation usually exhibit high stability for days or even months without adding surfactants.[21,22]

Numerous researches have been carried out to reveal the mechanism hidden in such a simple nanoprecipitation process.[18,23] Formation of nanoparticles through nano-precipitation is kinetically controlled. Supersaturation leads to the formation of numerous nuclei that can follow two fates: i) at low supersaturation, they grow further by incorporating some still-dissolved solute from the surrounding, called ‘Nucleation and Growth’ process; whereas ii) at high supersaturation, nuclei aggregate with each other in a ‘Nucleation and Aggregation’ process. Both processes robustly produce on-demand NPs albeit of different particle size and dispersity.

Practically, batch nanoprecipitation is the simplest mixing process by one-step or dropwise addition of the polymer solution into a large amount of non-solvent. Continuous processes (flash [23,24] and microfluidic [25] nanoprecipitations) can induce extremely fast and reproducible mixing times (less than a millisecond). These techniques share the same principle as the batch one, i.e. ensuring good control of the size and size distribution in an easy and reproducible manner but also afford continuous synthesis for

targeting larger productions; for more details on these various mixing devices used in nanoprecipitation, a review has been published in 2020.[26]

Triangle solute/solvent/non-solvent ternary phase diagrams are practical tools to study nanoprecipitation. They allow predicting the phase behavior of the solution after the solvent-shifting procedure (**Figure 1A**).[27,28] Once the compositions cross the binodal curve, spontaneous emulsification occurs, making this system transit from single phase to multiple phases. The spinodal curve defines the thermodynamic stability limit, beyond which phase demixion occurs. In between, a narrow metastable region exists where monodisperse suspensions are generated through nanoprecipitation. This area is coined “Ouzo region”. In order to conveniently visualize and study this tiny domain of composition, ternary phase diagrams can be transformed into binary ones by plotting the final mass fractions of solute and solvent as X- and Y- axes, respectively (**Figure 1B**) and applying a log scale to the X-axis to enlarge the Ouzo region.[17,29,30]

In the process of NPs formation, the driving force of the nanoprecipitation is the supersaturation of polymer in mixed solution. Hence, many key structural features of polymers required for other techniques, for instance, appropriate amphiphilic character, presence of ionic charges or others, are not decisive in this emulsification process. Accordingly, nanoprecipitation has been successfully applied to a wide range of polymers, including widely-used hydrophobic synthetic homopolymers such as polystyrene (PS),[31] poly(methyl methacrylate) (PMMA),[32] as well as biodegradable polymers, e.g. poly(ε-caprolactone) (PCL),[28] poly(glycolic acid) (PLA),[33] or poly(lactide-*co*-glycolide) (PLGA).[30] Polymers for sensing applications, i.e. Aggregation-Induced-Emission (AIE) polymers,[34] and semi-conducting polymers [35]

have also been nanoprecipitated. On the other side of the polarity scale, hydrophilic polymers such as proteins [36,37] or polysaccharides and their derivatives [22,38,39] are also amenable to nanoprecipitation.

In view of generating colloids with complex internal morphologies, nanoprecipitation can be engaged with mixtures of incompatible homopolymers or with microphase-separating block copolymers, where the 3D confinement-induced self-assembly promotes unconventional polymer rearrangement within the particle. Various nanostructured colloids of interest, e.g. porous, Janus, multifaceted, lamellar stacked, onion-like and core/shell NPs have been obtained by this manner. For some morphologies, the final state of polymer nanoparticles is not at thermodynamic equilibrium but rather kinetically frozen. Particle organization and shape under 3D confinement are strongly impacted by the confining strength (particle size vs chain length) and interfacial energies (between the polymer blocks and between the NP and the surrounding liquid phase). Meanwhile, polymer-solvent interaction, molecular weight and concentration of polymer(s) and temperature of the system determine the diffusion processes inside the particle, which further regulates the confined polymer assembly. Hence, the construction of NPs with complex morphologies requires precise identification of structural information and physicochemical properties of components, with a view to achieving a control of the final morphology.

The nanoprecipitation process has given a significant impulse to the construction of polymeric nanoparticles with controlled morphologies. Among them, thanks to repulsion between hydrophobic and hydrophilic segments, solvent shifting enables the self-assembly of amphiphilic copolymers into core/shell particles (i.e. micelles, vesicles,

liposomes, polymersomes, fibers, and so on).[40,41] Research on this topic has been exhaustively reviewed in the last decades, so these studies will not be discussed in this review. In addition, many reviews have already come out to summarize the applications of conventional solid NPs prepared by nanoprecipitation,[18,26,34,42] but the research on the design of complex nanostructured PNPs was hardly reported so far. In this review, we specially focus our interest on the recent advances in the fabrication of polymeric colloids with complex internal morphologies by nanoprecipitation. The first part will emphasize the development of equilibrium (typically onion-like) or non-equilibrium (stacked lamellae, porous) morphologies prepared from single colloidal components (mono-component PNPs). In the second part, we will focus on the versatility of the nanoprecipitation (batch or continuous) process in generating multi-faceted and core/shell morphologies by simultaneously or sequentially nanoprecipitating multi-component starting materials (multi-component PNPs). Here the components should be supersaturated in the solution for participating in the PNPs production after the solvent-shifting process and contribute to constructing the complex internal morphologies capable of being visible in the images. Typically, the PNPs generation relies on the absorption of surfactant-like molecules on the preformed PNPs rather than precipitation and on the encapsulation of functional molecules but without distinct core structure are also excluded from this review.

2. Mono-component PNPs

Compared to conventional self-assembly or emulsification technique that involves the use of surfactants to stabilize the particles, nanoprecipitation only requires a (homo- or

co-) polymer and a miscible solvent/non-solvent mixture to generate colloids through a straightforward solvent-shifting step. The synthesis of mono-component PNPs displaying different morphologies through nanoprecipitation is described in this part and the corresponding references compiled in **Table 1**. Thanks to the distinct physico-chemical features of polymers, porous and complex internally structured nanoparticles can be obtained through batch or flash nanoprecipitation.

2.1 Porous nanoparticles

Porous nanoparticles made of single polymer component have been developed by nanoprecipitation. Current research focuses on the self-assembly of hydrophobic carboxyl-functionalized polymer. The formation mechanism of the pores or the cavities in the particles is still unclear and may result from water swelling of amphiphilic parts of the polymer phase or/and phase separation into 'pools' by electrostatic interactions between groups.

By preparing NPs from benzoic and methacryloyl bifunctionalized dextran (**1**, **Chart 1,** MW of dextran ~35-40 kg/mol, degree of substitution ~0.64-1.44) through addition of THF solution into water (THF/water=1/2, v/v) and subsequent solvent removal process at 40°C, Weiss and coworkers surprisingly observed a distinct cavity at one side of the NPs without explaining the cause of this structuration (**Figure 2A**). In contrast, plain spheres were obtained by using acetone instead of THF.[21] Ma *et al.* observed porous nanospheres (called "dimpled beads") generated from batch nanoprecipitation of hydrophobic AIE polymers poly(1,1,2,2-tetraphenylethene) (**2**, **Chart 1**) by using THF as solvent (final THF/water=1/9, v/v) (**Figure 2B**).[43] The particle size increased from

about 170 to 200 nm with increasing polymer chain length (molecular weight ranging from 2.5 to 12 kg/mol). The AIE NPs internalized in Hela cell showed a strong blue fluorescence for an excitation at 405 nm. In addition, Vu and coworkers have also constructed anisotropic nanoparticles (~250 nm) with a single cavity by 'one-shot' adding THF solution of polystyrene (**3, Chart 1**) into water (THF/water=1/4, v/v) [44]. Seen from these works, the morphology of dimpled beads is invariably obtained from self-assembly of very different polymers, i.e. either amphiphilic polysaccharide derivatives or extremely hydrophobic (homo)polymers. Note that the mechanism for pore formation in the particles is still not clear, even if the conditions of preparation advise for a structure at equilibrium (slow removal of solvent at 40°C).

Recently, Hu *et al.* took advantage of flash nanoprecipitation and post-chemical reactions to produce a series of carboxyl-functionalized PS-based (**4**, **Chart 1**) porous nanoparticles (~ 210 nm) in THF/water mixture. $NaBH_4$ introduced in the water reservoir not only deprotonated the carboxyl groups but also catalyzed Ag^+ reduction reaction after fast mixing of polymer THF solution and $AgNO_3$ aqueous solution in a confined impinging jet (CIJ) mixer (THF/water/water reservoir=1/1/10, v/v/v) (**Figure 2C**). It is worth mentioning that the CIJ mixer, in which two streams of solvent and non-solvent at equally high velocity rapidly mix in the microchamber, has been widely used for flash nanoprecipitation. The particles swelled in aqueous solution owing to the presence of highly hydrophilic carboxylate groups and water pockets grew within the polymer phase resulting in the formation of multiple cavities at the core of the particles. Meanwhile, the surface of particles was coated *in situ* with Ag NPs.[45] These metal NPs distributed in PS matrix (Ag content, 2.7 wt%) were found capable to efficiently catalyze the reduction

of 4-nitrophenol by $NaBH_4$ to 4-aminophenol.

Jiang and coworkers systematically investigated the impact of pH on the formation of porous nanostructures from carboxyl-terminated polyimide (**5**, **Chart 1**, 3.6 kg/mol).[46] All nanoparticles were prepared by dropping pH-adjustable aqueous solutions into polymer/THF solution (THF/water=1/9, v/v, **Figure 2D**). At pH 8, only a small amount of carboxyl groups is deprotonated, so that broadly distributed “dimpled beads” with a size ranging from 100 to 600 nm were obtained after nanoprecipitation (**Figure 2E**). When the pH was increased to 10, more deprotonation took place leading to porous nanoparticles of smaller sizes (100-200 nm, **Figure 2F**). The mobility of the polymer chains seems to be of crucial importance in the formation of porous nanostructures as low-T_g’s carboxyl-ended polybutadiene chains self-assembled exclusively into conventional spheres at different pHs.

2.2 Complex internally structured nanoparticles

Confined self-assembly of block copolymers with incompatible segments have been proven to robustly and scalably produce various PNPs of complex morphologies after emulsification and solvent removal.[47,48] As a general process, polymer colloids are generated through ~~a~~ surfactant-assisted emulsification, followed by a post-evaporation step to trigger orderly reorganization of copolymers in the particles. In stark contrast to this conventional method, surfactant-free nanoprecipitation of block copolymers directly leads to microphase separation inside the particles after solvent-shifting. The rearrangement of the polymer chains under 3D-confinement (with or without solvent evaporation) results in a rich variety of internal morphologies.

In their pioneering works, Yabu, Higuchi and Shimomura introduced the formation of polystyrene-*block*-polyisoprene (PS-*b*-PI, **6**, **Chart 2**) based nanoparticles through a nanoprecipitation and post-evaporation method.[49] In the approach developed by the authors, water is progressively added into a copolymer/THF solution while stirring, with final volume ratios of water/THF fixed at 1/1 or 2/1. Although some dispersions look transparent due to high dilution of polymer concentrations (lower than 0.2 g/L), still some particles are generated by the nucleation and growth process at this low supersaturation level.[50] Long THF evaporation time is required to favor the diffusion and reordering of the polymer chains in the particles, resulting in a variety of complex internal nanostructures, typically stacked lamellar or onion-like (*vide infra*). This method was coined as Self-ORganized Precipitation (SORP, **Figure 3A**).[51]

In 2005, stacked lamellar nanoparticles were first generated by SORP (THF/water =1/1, v/v) of PS_{171}-*b*-PI_{176}, which was attributed to the microphase separation of this block copolymer within the particles (**Figure 3B-D**).[52] The thickness of the PS and PI layers were 11.0 and 11.9 nm, respectively. Note that the size of the resulting particles was not mentioned in this work. In contrast, nanoparticles with bicontinuous phase were obtained by rapid batch nanoprecipitation, which stresses the importance of the evaporation step in block copolymer organization in such a confined geometry.

In general, slow dropwise-mixing process and post-evaporation step of SORP favor the confined evolution of block copolymer association towards the equilibrium state. Meanwhile, an increase of polymer viscosity and a decrease of manipulation temperature can hinder this morphological transition and “freeze” the intermediate nanostructures in an out-of-equilibrium state, resulting in a series of original

morphologies.

The impact of the molecular weight of copolymers on the final nanostructures was investigated by nanoprecipitating PS-*b*-PI copolymers of increasing MW of 30, 76, 266 and 1550 kg/mol, the relative fraction of PI segment in the copolymer ranging between 0.43 and 0.58.[53] The size of the resulting particles increased with molecular weights as evidenced by transmission electron microscopy (TEM) photos. Pure well-ordered stacked lamellar nanoparticles were obtained starting from block copolymers of 30 and 76 kg/mol in molar masses, with periods of lamellae of 23 and 34 nm, respectively. Increasing polymer molar mass increased the lamellae period and widened the diversity of resulting nanostructures, including single lamellar Janus structure and non-lamellar patchy structures. This may stem from high viscosity and low diffusion rate of high molar mass polymer chains that preclude this system from reaching the equilibrium state. For MW of 1550 kg/mol, no stacked lamellar particles were observed. The internal structure of the NPs was also proven to vary with the relative length of the PI block in the copolymer.[54] By decreasing the volume ratio of PI to 0.28 (MW of 51 kg/mol), the copolymer self-assembled into hexagonally-packed cylindrical structures within the particles.

The importance of the temperature applied for THF removal was also evaluated (**Figure 3E**).[55] Here, an increase of temperature promotes molecular diffusion, favors interactions between polymer and solvent and decreases the viscosity, promoting polymer rearrangement in the particles to reach thermodynamic equilibrium. At 10°C, there was insufficient energy for molecular reshuffling and similar disordered nanostructures as the ones observed in batch nanoprecipitation. By increasing the

temperature to 25°C, stacked lamellar nanospheres were robustly produced. When the temperature was set at 40°C, the internal morphology evolved from stacked lamellar to onion-like organization, suggesting that the latter is at thermodynamic equilibrium. Since PI block has a slightly higher water affinity over the PS block, the PI segment covered the onion-like particles as an outmost layer to reduce the interfacial tension between the particles and water. Consistent with this assumption, evaporation by microwave annealing (at a frequency of 700 W) resulted in fast phase reorganization so that only 2 min were necessary for the morphology to transform into an onion-like nanostructure.[56]

Recently, Yabu and Delaittre investigated the SORP of PS-*b*-PI having a very small amount (~6% molar ratio) of 4-vinylbenzyl chloride (VBC) or pentafluorostyrene (PFS), into the PS block (P(S-*co*-VBC)-*b*-PI and P(S-*co*-PFS)-*b*-PI, $M_{n,NMR}$=48.9 and 47.3 kg/mol prepared by nitroxide-mediated copolymerization, f_{PS}=0.47 and 0.50, see structures **7** and **8** in **Chart 2**).[57] Azide moieties were post-incorporated into the polymer chains by nucleophilic substitution of chloride (in vinylbenzyl chloride moieties) with sodium azide (P(S-*co*-VBA)-*b*-PI, $M_{n,NMR}$=48.8 kg/mol, f_{PS}=0.47, **9**, **Chart 2**). Performing SORP on polymers at different solvent ratios (water:THF=1:3, 1:1, 3:1) and concentrations (0.1 and 1 mg/mL) afforded a series of internally phase-separated PNPs. P(S-*co*-VBC)-*b*-PI and P(S-*co*-PFS)-*b*-PI-based NPs shared similar size ranging from 140 to 300 nm (with no clear trend in the evolution of NPs with concentration and solvent ratio). In contrast, P(S-*co*-VBA)-*b*-PI-based NPs bearing polar azido groups showed a relatively high affinity to the solvent, so that the particle size (in a range from 200 nm to 3 μm) grew by increasing the content of THF. A stacked lamellae morphology was only

observed at a concentration of 0.1 mg/mL for P(S-*co*-VBC)-*b*-PI and P(S-*co*-VBA)-*b*-PI-based NPs, while P(S-*co*-PFS)-*b*-PI with hydrophobic PFS moieties formed onion-like morphology in different conditions. Interestingly, the carboxyl end groups attached to the extremity of the PS block favor the presence of such blocks at the particle/water interface and the formation of onion-like nanostructures with a PS top layer.

Zhang and coworkers also fabricated a series of complex internally-nanostructured nanoparticles through dropping water into a fluorine-containing block copolymer solution, poly(*tert*-butylacrylate)-*b*-poly(2-[(perfluorononenyl)oxy]ethyl methacrylate) ($PtBA_{90}$-*b*-$PFNEMA_{12}$, **10**, **Chart 2**).[58] Solvent evaporation was not required here to favor polymer reorganization within the particles. Increase of water content (from 50 to 80 vol.%) and decrease of temperature (from 40 to 10 °C) led to an enhancement of the incompatibility between the two blocks. Microphase separation and reduction of the molecular mobility during chain rearrangement produced a series of out-of-equilibrium intermediate PNPs morphologies. It resulted in transitions of both surface and inner morphologies of particles from ordered (stacked lamellar inner, onion-like outer, 40 °C, 50 vol% of water) to disordered patterns (twisted striped surface and disordered inner structures, 10 °C, 80 vol% of water, see **Figure 4A**).

Similar nanostructures were constructed by Priestley and Panagiotopoulos using the flash nanoprecipitation technique.[59] Streams of THF solution of PS-*b*-PI and water were mixed in a CIJ mixer and finally diluted in a water reservoir (THF/H_2O stream/H_2O reservoir =1/1/1, v/v/v, **Figure 4B**). Using low MW (27 kg/mol) symmetrical copolymer, stacked lamellar nanoparticles were obtained. The diameters ranged from 30 to 300 nm

with an increase of polymer concentration, whereas the period of lamellae was around 18.2 nm for all concentrations. Increasing the polymer MW (~225 kg/mol) led to a disordered lamellar morphology, with lamellae period of 71 nm (large particle size distribution, 200~700 nm). All the values were in agreement with molecular dynamic (MD) simulations. Three stages of phase separation were observed in the simulation, including microphase separation, domain coarsening and defect annealing (**Figure 4B**). In the case of high MW copolymers, the glassy PS block significantly slowed down the defect annealing and limited the phase separation resulting in the formation of a disordered lamellar structure.

3. Multi-component PNPs

Apart from structured mono-component PNPs, blends of (mostly polymer) solutes displaying distinct structural and/or physicochemical characters can be nanoprecipitated together into multi-component particles. The phase separation occurring between incompatible components in the particles promotes the formation of a myriad of morphologies including principally multi-faceted and core/shell nanoparticles (see a full compilation of the results discussed below in **Table 2**).

3.1 Multi-faceted nanoparticles

Janus nanospheres are the simplest faceted particles with two discernible hemispheres. In order to complete the assembly of two hemispheres, Smith and coworkers designed a specific fluidic nanoprecipitation device (**Figure 5A**).[60] Two PLGA polymers (**11, Chart 3**) of different compositions (PLA/PGA=3/1 and 1/1) were fully dissolved in DMF and acetone, respectively. Two polymer solution streams (1 mL)

were then equally exposed to water stream (40 mL) by a pair of side-by-side inlet channels, leading to the formation of Janus nanoparticles. By pre-dissolution of Nile red and rhodamine in DMF and acetone, respectively, the two probes were finally encapsulated in their respective polymer domains. The Janus morphology was confirmed by the detection of two distinct spatially-resolved fluorescence signals in the particles.

Higuchi *et al*. prepared Janus nanoparticles through SORP of PS and PI (**12**, **Chart 3**) mixtures.[54] Homopolymers of PS (17 kg/mol) and PI (12 kg/mol) were dissolved together in THF. The nanoprecipitation of the two polymers simultaneously took place through solvent shifting process (THF/water=1/2, v/v). The incompatibility between PS and PI triggers a phase separation inside the particles. As the two polymers have similar 'affinity' for water-rich solutions (very close solubility parameters for PS and PI), the homopolymers self-organize into two phase-separated domains within the particles for reduction of the interfacial energy between the polymer domains (**Figure 5B**). The volume of the two spherical caps correspond to the contents of each homopolymer in the feed. To further extend the library of Janus NPs, PS-*b*-PI block copolymers (29.8, 51.2 and 86 kg/mol, volume fractions of PI were 0.51, 0.28 and 0.51) were added to mixtures of homopolymers (PS:PI:PS-*b*-PI=1:1:0.6 in wt.) to modulate the interfacial energy between PS and PI domains. When the MW of the blocks in the symmetrical copolymer was similar to those of the homopolymers, the interfacial energy was significantly decreased, resulting in the formation of patchy nanostructures. Increasing the MW of the glassy PS block altered the compatibilization of the two phases, so that Janus particles with ultrasmall PI spherical domains in the PS phase were then formed (**Figure 5B**). The

authors also blended PS-*b*-PI (M_n = 230 kg/mol, f_{PI}=0.47, 0.58) with asymmetric copolymers poly(isoprene-block-2-vinylpyridine)(PI-*b*-P2VP, M_n = 32, 92 kg/mol, f_{P2VP}=0.27, 0.15, **13**, **Chart 3**) or poly(styrene-block-2-vinylpyridine) (PS-*b*-P2VP, M_n = 27, 338 kg/mol, f_{P2VP}=0.33, 0.35, **14**, **Chart 3**) through SORP process.[61] A series of complex internally nanostructured PNPs were then obtained: specifically, PS-*b*-PI was conanoprecipitated with 25 wt% of high molecular weight PI-*b*-P2VP leading to the formation of onion-like morphology, while a cylinder phase was observed in the particles by blending with 25 wt % low molecular weight PI-*b*-P2VP. Similar microphase separation was observed when the PS-*b*-P2VP was introduced at the same weight ratio. Finally, a very interesting morphology, Janus PNPs containing a lamellar PS-*b*-PI phase and a packed cylindrical high MW PI-*b*-P2VP phase, was prepared by SORP of the two polymers at equal weight fraction. Recently, the same authors blended together three different synthetic functional copolymers P(S-*co*-VBC)-*b*-PI, P(S-*co*-VBA)-*b*-PI and P(S-*co*-PFS)-*b*-PI (48.9, 48.8 and 47.3 kg/mol, volume fractions of PS of 0.47, 0.47 and 0.50) with PS-*b*-PI (similar M_n and f_{PS}, 43 kg/mol and 0.48).[57] A stacked lamellar morphology was observed at 1:1 weight ratio of the PS-*b*-PI/functional copolymers. The PI segments of P(S-*co*-PFS)-*b*-PI/PS-*b*-PI blend-based stacked lamellar NPs was further crosslinked by osmium oxide (OsO_4). Flat nanodiscs containing a disc-shaped PI core and a pentafluorophenylalkyl functionalized PS shell were then obtained by disentangling the PS domain through redispersion of solid particles in THF.

Priestley and Prud'homme systematically investigated the formation of multi-faceted morphologies through flash nanoprecipitation.[59,62-64] Nikoubashman and Panagioto-poulos reported on the molecular dynamics simulations of the

process.[65-67] Experimentally, homopolymers (PS, MW~16.5 kg/mol and PI, MW~11 kg/mol) were simultaneously nanoprecipitated in the solution after ultrafast mixing of THF solution and water in a CIJ mixer (THF/H_2O/water reservoir=1/1/1, v/v/v). PI and PS showed extremely low surface tensions between each other compared to those between each polymer and water. After co-nanoprecipitation of the two polymers in the solution, Janus nanoparticles were built at low PS/PI weight ratios (1/4 and 1/1, see morphology transition in **Figure 6A**).[62] The glassy polystyrene actually acts as a trapping agent promoting the formation of non-equilibrated structures. The vitrification of PS in the particles restrained morphology transition to reach equilibrium and enabled to freeze the intermediate architectures in the molecular rearrangement to Janus configuration. Increasing its content in the feed led to multi-faceted morphology (**Figure 6A**). Increase of concentration and/or molecular weight of homopolymers slowed down the phase separation and shortened the vitrification time, resulting in frozen multi-faceted particles. The impact of polymer chain mobility was also explored by heating the suspension of multi-faceted NPs to 95°C (T_g of PS is 100°C). The mobility of PS chains in the particles was enhanced to trigger a morphology transition to Janus nanoparticles (**Figure 6B**).[63] Addition of a non-ionic surfactant, Tween 80 (**Figure 6C**), in PS/PI system reduced the interfacial energy of o/w interface, leading to the formation of snowman-like morphology.[64] Blends of PS (MW~1500 kg/mol) and block copolymer PS-*b*-PI (MW~27.3 kg/mol) through flash nanoprecipitation led to more complex multi-faceted nanoparticles composed of one bulky PS phase and one or more lamellar block polymer phases (depending on the concentration of polymers and volume fraction of homopolymer PS, **Figure 6D**).[59] All results were in agreement with MD simulations,

showing that surface tensions between polymers and between each polymer and solvent, are the most decisive parameters for predicting the equilibrium morphology.

Recently, PS (16 kg/mol), PI (11 kg/mol) and an amphiphilic block copolymer PS-*b*-PEG (relative volume of the PEG block in the copolymer varied from 0.1 to 0.8, 6.6-8.8 kg/mol) were co-nanoprecipitated into Janus nanoparticles using a CIJ mixer (THF/H_2O=1/1 v/v). [68] Amphiphilic copolymers preferentially absorbed onto PS hemispherical surface to minimize the surface energy. The diameter of particles decreased gradually with an increase of copolymer content (from 0 to 50 wt%). Meanwhile, the zeta potential of particles increased from -26 to -5 mV, which was attributed to the formation of a PEG corona. Both the volume of PEG block and block copolymer content influenced the resulting morphologies. Increase of hydrophilicity (relative volume of PEG block above 0.39) at high content of block copolymers (50 wt%) led to a morphological transition to core/shell nanoparticles stabilized by a PS-*b*-PEG membrane (**Figure 6F**). The amphiphilic Janus NPs strongly adsorbed at a decane/water interface to generate a Pickering emulsion with droplet stability of more than 3h. These NPs were more effective stabilizer than the hydrophobic PI-PS Janus NPs. The flash nanoprecipitation method has been proven to adapt universally to various polymers, i.e. PLA (11 kg/mol), poly(butadiene) (PB, 18 kg/mol), poly(vinylcyclohexane) (PVCH, 25 kg/mol) (**15**, **16** and **17**, **Chart 3**). Taking advantage of the incompatible characters among each other (PB and PS, PS and PLA, PB and PLA, PB and PVCH), the straightforward nanoprecipitation process allowed constructing a variety of binary (PB-PS, PS-PLA, PVCH-PB, and PB-PLA) Janus or even ternary (PS-PB-PVCH) Cerberus PNPs with on-demand compositions, properties, and functionalities.

3.2 Core/Shell nanoparticles and nanocapsules

Two nanoprecipitation strategies allow preparing core/shell nanostructures:

i) sequential or successive nanoprecipitations that take advantage of distinct solubility difference among the solutes. The selective nanoprecipitation of the molecules in sequence by progressive additions of different contents of non-solvent leads to a core/shell structure. Purification is not required here between successive additions;

ii) conanoprecipitation, where all solutes are simultaneously nanoprecipitated and phase-separate in the particles. Distinct polymer-solvent interactions promote the rearrangement of molecules in a defined radial sequence, achieving the formation of a core/shell nanostructure.

3.2.1 Solid-core nanoparticles

Chambon *et al.* constructed core/shell NPs (diameters of 77-85 nm) by successive batch nanoprecipitation of organic semiconductor materials poly(3-hexylthiophene) (P3HT, 40 kg/mol) and [6,6]-phenyl-C_{61}-butyric acid methyl ester (PCBM) (**18** and **19**, **Chart 4**).[69] The two precursors were pre-dissolved in THF. Addition of DMSO into THF solution (DMSO/THF=9/1, v/v) selectively nanoprecipitated P3HT into core NPs (diameter of 68-83 nm). Further addition of water (water/DMSO=9/1, v/v) induced the supersaturation of PCBM and its precipitation at the interface, forming PCBM shell around the core NPs (**Figure 7A**).

Santos and Liu designed a specific microfluidic device for superfast sequential nanoprecipitation process (milliseconds intervals between sequential steps).[70] The device consisted of three input streams, including (1) an organic solution containing both core and shell precursor molecules (F1), (2) a non-solvent for core molecules (F2) and (3)

a non-solvent for core and shell molecules (F3). Practically, the core molecules (anticancer drug paclitaxel, sorafenib or PLGA) were precipitated into core NPs by ultrafast mixing of streams of acetone solution and aqueous solution at pH 10.5. The polymer shell based on hypromellose acetate succinate (**20**, **Chart 4**), pre-dissolved in acetone solution with the core molecules, was precipitated by a pH shifting process. Basically, an acidic aqueous solution (pH 4) stream triggered the supersaturation of the shell polymer by screening the polymer charges, resulting in core/shell nanoparticles (flow ratios of F1/F2/F3=1/2/6 or 1/5/30) (**Figure 7B**).

Shimomura and Yabu prepared PI@PMMA (core@shell) particles through SORP process.[71] PI (12 kg/mol) and PMMA (15.8 kg/mol, **21**, **Chart 4**) were co-nanoprecipitated in THF/ water mixture (1/2, v/v). In stark contrast to PI and PS mixtures whose close solubility parameters promoted the formation of Janus NPs, the water affinity of PI was lower than that of PMMA which then forms the outermost layer of the NPs. This result confirms the significant role of interfacial tensions between the homopolymers and the surrounding liquid in NP internal structuration. The size of core/shell nanoparticles increased from 273 to 372 nm by increasing the polymer concentration from 0.05 to 0.3 g/L (weight ratio of PMMA/PI=1/1). This method was also applied to generate PIB@PI (polyisobutene, PIB, 19.5 kg/mol, **22**, **Chart 4,** PI, 138 kg/mol) and PS@PMMA (PS, 131 kg/mol, PMMA, 15.8 kg/mol) NPs.[72]

Flash conanoprecipitation (using a CIJ mixer, THF/water/water reservoir =1/1/1, v/v/v) was applied by Priestley *et al.* to produce PI@PS-NH_2 nanoparticles using PS-NH_2 (10 kg/mol) and PI (11.6 kg/mol). [64] In contrast with nanoprecipitation of conventional PS/PI mixtures which result in the design of Janus NPs, the presence of terminal amine

groups on the PS chains led to the preparation of NPs with a PI core and a PS shell.

Zhao and workers were committed to developing core/shell PNPs of high drug loading through nanoprecipitation for biomedical applications. To do so, a sequential nanoprecipitation was introduced by Zhao and Weitz to supersaturate drugs and polymers in sequential order for encapsulation.[73] Different from general nanoprecipitation using a single solvent, a trinary solvent mixture of DMSO, DMF and ethanol was employed for dissolving a series of hydrophobic drugs (i.e. curcumin, paclitaxel, ibuprofen, docetaxel and amphotericin B) and biocompatible polymers including shellac (**23**, **Chart 4**) and PLGA-*b*-PEG (**24**, **Chart 4**, 25 and 60 kg/mol), that effectively inhibited the spontaneous crystallization of the drugs after the solvent-shifting process. Taking curcumin@shellac NPs as an instance, upon adding the first round of PBS buffer at pH7.4 (organic solvent/PBS buffer=1/1, v/v) into the solvent mixture (DMSO/DMF/ethanol=4/3/3, v/v/v), curcumin was selectively nano-precipitated into small aggregates with a diameter of 40 nm. Second round addition of the same volume of PBS buffer induced the precipitation of shellac at the interface for encapsulating the drug NPs, resulting in stable core/shell NPs (diameter of 50 nm) with an encapsulation efficiency of up to 99% and loading capacity of up to 50%. This process also allows the generation of more versatile PNPs by simultaneously nano-precipitating multiple polymers in the second solvent-shifting step for adjusting the release manner of the polymer membrane. In contrast to the significant swollen and rapid drug release profile of shellac shell, the polymer shell consisting of PBLG-*b*-PEG and shellac (1/1, wt/wt) maintained the morphology and slowed down the release at 37 °C, exhibiting a sustained release over 7 days. The paclitaxel@shellac and PBLG-b-PEG mixed NPs with a high drug loading of

39.6% performed much better anti-tumor therapeutic effects in vitro and in vivo than the ones with a drug loading of only 3.5%.

In addition, Zhao also constructed high drug loading core/shell PNPs through microfluidic nanoprecipitation. The conventional 2-dimension microfluidic approach afforded curcumin-loaded PNPs with a loading capacity of only ~4%.[74-75] Zhao and coworkers fabricated a 3-dimension microfluidic device capable of minimalizing the NPs absorption on the channel surface for solving the aggregation-clogging issue.[76] The ternary solvent mixture stream (DMF/DMSO/Ethanol=3/4/3, v/v/v) containing curcumin and shellac went through a needle inner channel to rapidly mix with water or aqueous solution stream in a tubular outer channel. This solvent-shifting process led to simultaneous nanoprecipitation of the drug and polymer to self-assemble into curcumin@shellac nanoparticles, that attributed to the higher affinity of shellac to water. The diameter of the PNPs with a maximal loading capacity of ~50% could be conveniently mediated in the range of 86~142 nm by adjusting the initial curcumin concentration (20~57%) and flow ratios (0.034~0.2). Tuning the pH from 4.5 to 7.4 induced the swelling of the shellac membrane, that significantly decreased the colloidal stability of the NPs and accelerated the curcumin release in the solution.

3.2.2 Oil-filled nanocapsules

Hydrophilic core/shell NPs that consist of an extremely hydrophilic shell and a hydrophobic core, can be also straightforwardly generated by nanoprecipitation. To achieve this, upon mixing of the two phases, a hydrophilic polymer first dissolved in water is precipitated at the same time as the hydrophobic oil incorporated in organic

solvent. Solvent shifting conditions are chosen so that the hydrophilic polymer chains stick preferentially at the o/w interface after phase separation and cover the organic NPs or nanodroplets to produce core/shell nano-objects in one pot. In order to trigger simultaneous co-nanoprecipitation of the hydrophilic polymer and hydrophobic molecule, it is thus required to carefully establish and overlap the phase diagrams of hydrophilic polymer and hydrophobic molecule/organic solvent/water systems (**Figure 8**) for precisely locating the appropriate conditions of solvent shifting. The cloud point boundary indicates the solubility limit of the hydrophilic polymer. Supersaturation takes place when crossing this line.

The so-called 'Shift'N'Go' process that we extensively studied has allowed generating a library of nanocapsules (NCs) with different features and properties. We summarize here what can be achieved with different water-soluble polymers in terms of NCs structures (e.g. size of the objects, thickness, density and functionality of the shell, colloidal stability) and features (tailored or diffusion-controlled release, biodegradability, storage, cell toxicity). For the records, most of the synthetic polymers involved in the construction of the nanocapsules' membrane were prepared by RAFT polymerization (poly(N-[7-(α-D-mannopyranosyloxy) heptyl] methacrylamide) (PHMM, **25**, **Chart 5**),[77, 78] poly(N-[2-(α-D-mannopyranosyl-oxy)ethyl] methacrylamide) (PEMM, **27**, **Chart 5**),[29] poly(N-(2-hydroxypropyl) methacrylamide) (PHPMA, **28**, **Chart 5**)[79]) and copolymers of these (**26**, **29**, **30**, **31**, **Chart 5**). Importantly, commercial polymer dispersants [80] (Pluronic, PVA), polysaccharides [81] (dextran and derivatives, pullulan, glycogen, hyaluronic acid, **32**, **33**, **34**, **35**, **36**, **Chart 5**) and proteins (suckerin-based peptides) [82] have also been used with success.

The size range of nanocapsules depends on the domain of the phase diagram considered: in the Surfactant-Free MicroEmulsion (SFME) domain, one can generate capsules as low as 40 nm in diameter (PEMM) but most likely into the 80-200 nm range. In the Ouzo domain, NCs sizes are generally smaller when using synthetic glycopolymers (around 120 nm) but rather come out as 200 to 500 nm when considering polysaccharides, the larger nanocapsules being observed for the most hydrophilic pullulan. As the size of oily core (at same concentration) is the same whatever the nature of the polysaccharide, the disparities in size between these systems mainly come from distinctive swelling behavior of the polymeric shells. The size distribution is rather low in all case (PDI of less than 0.2) whatever the process. This particle size range (typically below 200 nm) is compatible with applications in nanomedecine.[18] Besides, the presence of ionic charges along the polymers chains has a drastic influence on the PNPs size. The presence of charges favors the stabilization of oily droplets, but it may disturb the polymer deposition at the water/acetone-oil interface, resulting in the formation of undesired small-sized polymer aggregates and thin-layered nanocapsules in the suspension. Hence, when a mixture of neutral and charged polymers (10-30 wt% of charged polymers) was used for nanoprecipitation, simultaneous deposition of the polymer chains and early stabilization of aggregated nuclei produced exclusively monodisperse nanocapsules with dimensions around 100 nm in diameter.

The molar mass of the polymers strongly affects the cloud point boundaries. The domain where co-nanoprecipitation of oil and polymer is achievable can then be significantly enlarged or shrunk depending on the solution properties of the polymer to be used. Oligomeric glycopolymers or polysaccharides generally show enhanced

solubility in acetone/water mixtures (up to 80 wt% acetone), whereas polymers of higher MW rapidly reach a threshold around 30 to 40 wt% acetone (for polysaccharides) and slightly larger for synthetic dispersants and glycopolymers (50 to 60 wt%). For highly hydrophilic polymers, a double crosslinking step is advised in order to increase the crosslink network density. The conclusion here is that capsules can be designed from any type of water-soluble reactive polymers (or mixture of these) as long as (the) phase diagram(s) is (are) known. A large range of oils can be used for the construction of the core.

We have also shown that the functionality of the polymer shell is tunable at will. For instance, making use of available hydroxyl groups (on the sugar groups, but also on PVA) or reactive groups introduced on purpose (such as epoxides) allows crosslinking and decorating the shell with molecules of biological interest (fluorophores, biotags such as biotin or folic acid, stealth agents such as PEG, magnetic metallic nanoparticles). Besides, one can increase the thickness and change the nature of the outermost layer by carrying out sequential precipitations on the NC surface, up to 3 rounds (**Figure 9**).[81, 83] Negative (carboxylic or sulfate groups) and positive (quaternary amine groups) charges can be introduced by playing with the nature of the (co)polymer and sequence of precipitation.

Last but not least, the NCs can also be loaded with interesting actives such as drugs and/or fluorophores. The limit here is the solubility of the actives in the chosen oil constituting the core, so that bulk precipitation of active is preferred. We have done that recently with AIE molecules,[80] whose nano-confined crystallization in the core was initiated upon freeze-drying.

Most NCs comply with specifications for nanomedicine applications. Shell building and functionalization bring a transport ability in body fluid (charge of surface, PEG stealthness, brightness with fluorophores), the absence of toxicity and biodegradability (for polysaccharides, PHPMA and PVA), and a tunable release behavior (using sacrificial bonds issued from cystamine, for instance). Playing with multilayers and crosslinking density, impermeable to diffusion-limited releasing NCs can be reached. Powder state after freeze-drying allows long storage whereas NCs taken back in water or buffer retain their morphology and properties.

4. Conclusions and future outlook

This review has summarized important contributions of nanoprecipitation for the preparation of controlled nanostructured polymeric NPs. The simplicity of the process allows generic use of various polymers for the straightforward construction of a large range of structured nano-objects. The internal morphological ordering of the PNP can be precisely modulated by adjusting the physico-chemical characteristics of the macromolecular building blocks (*i.e.* incompatibility of the blocks, composition, molecular weight, glass transition temperature and so on), the interfacial energy between the polymers and the surrounding liquid phase, and the temperature.

Moreover, in stark contrast to conventional self-assembly using copolymers, surfactant-free nanoprecipitation allows a variety of incompatible homopolymers to be co-nanoprecipitated into multi-component particles. The facile ‘one-pot’ solvent shifting and the subsequent reorganization of the polymer chains within the confined nanoparticles simplifies the entire synthesis process, and gives access to a myriad of PNP morphologies such as Janus, multi-faceted, core/shell and so on. Nanoprecipitation

of block copolymers as single component or in combination with homopolymer blends further extends the library of nanostructured colloids.

Still today, the research on the synthesis of complex nanostructures via nanoprecipitation is at its infancy and does not permit to get the full picture and potentialities of such a versatile technique. So far, nanoprecipitation mostly led to the formation of spherical nanoparticles. Some interesting morphologies (shapes and/or internal nanostructures) obtained from other techniques (for instance, ellipsoids, cubosomes, hexosomes, honeycomb-like, and so on), often require more sophisticated polymer structures, components or conditions (i.e. triblock copolymers, specific surfactants, high shear force-induced emulsification, and so on). These have not been developed yet using the nanoprecipitation strategy and should definitively be addressed.

Besides, to further take the benefit of simple, straightforward, and versatile characters of nanoprecipitation, it would be valuable to explore diverse macromolecular systems (multiblock polymers, branched polymers, etc.) in the future. One interesting direction would be to impart stimuli-responsiveness to the particles. PNPs could be re-shaped in response to external triggers (i.e. light, heating, and so on) in a reversible rearrangement/recovery behavior. For instance, thermo-responsive PNIPAM that exhibits an LCST, or light-responsive polymers may be engaged in nanoprecipitation processes to construct smart nanoparticles. We envision these photo- or thermo-responsive particle rearrangements would endow PNPs with unconventional properties, thereby significantly expending the field of applications.

Finally, one could also give some attention to the influence of the mixing process involved in nanoprecipitation. The mixing rate of solvent and non-solvent has a

significant impact on the nucleation of NPs and diffusion of the polymers. This specific feature of the nanoprecipitation process could be usefully employed to modulate the resulting polymeric nanostructures by simply regulating phase flows. Batch nanoprecipitation is the most popular choice for solvent shifting thanks to its simple procedure, but this relatively slow solvent-exchange process (e.g. gradual solvent/non-solvent mixing) thermodynamically favors particle rearrangement towards the equilibrium state and prevent the capture of interesting transitional morphologies. Flash and microfluidic nanoprecipitation processes induce extremely rapid and precisely time-adjustable mixing and may allow the formation of original kinetically frozen nanostructures.[59] These continuous processes must be extensively spread and challenged in the future.

To summarize, we believe that there are appealing prospects for the synthesis of versatile PNPs with unprecedented nanostructures of new interesting shapes, external and/or internal nanostructures via nanoprecipitation, hopefully expanding their applications in a large range of fields.

Notes

The authors declare no competing financial interest.

Acknowledgements

X. Y. thanks the support from the National Natural Science Foundation of China (21902117) and the Natural Science Foundation of Tianjin (20JCQNJC01110).

References

[1] Elsabahy M, Wooley KL. Chem Soc Rev 2012; 41: 2545-2561.

[2] Kamaly N, Xiao Z, Valencia PM, Radovic-Moreno AF, Farokhzad OC. Chem Soc Rev 2012; 41: 2971-3010.

[3] Elsabahy M, Heo GS, Lim S-M, Sun G, Wooley KL. Chem Rev 2015; 115: 10967-11011.

[4] Ford WT, Miller PD. Microspheres, Microcapsules Liposomes 2002; 4: 171-202.

[5] Lyu Y, Pu K. Adv Sci 2017; 4: 1600481.

[6] Reches Y. Constr Build Mater 2018; 175: 483-495.

[7] Hasani-Sadrabadi MM, Majedi FS, VanDersarl JJ, Dashtimoghadam E, Ghaffarian SR, Bertsch A, Moaddel H, Renaud P. J Am Chem Soc 2012; 134: 18904-18907.

[8] Jana B, Ghosh A, Patra A. Photon Harvesting in Conjugated Polymer-Based Functional Nanoparticles. J Phys Chem Lett 2017; 8: 4608-4620.

[9] Ghosh Chaudhuri R, Paria S. Chem Rev 2012; 112: 2373-2433.

[10] Walther A, Müller AHE. Chem Rev 2013; 113: 5194-5261.

[11] Tan L, Tan B. Chem Soc Rev 2017; 46: 3322-3356.

[12] Giacomelli C, Schmidt V, Aissou K, Borsali R. Langmuir 2010; 26: 15734-15744.

[13] Fan X, Yang J, Loh XJ, Li Z. Macromol Rapid Commun 2019; 40: 1800203.

[14] Tritschler U, Pearce S, Gwyther J, Whittell GR, Manners I. Macromolecules 2017; 50: 3439-3463.

[15] Motornov M, Roiter Y, Tokarev I, Minko S. Prog Polym Sci 2010; 35: 174-211.

[16] Vitale SA, Katz JL. Langmuir 2003; 19: 4105-4110.

[17] Ganachaud F, Katz JL. Chemphyschem 2005; 6: 209-216.

[18] Lepeltier E, Bourgaux C, Couvreur P. Adv Drug Deliv Rev 2014; 71: 86-97.

[19] Schubert S, Delaney JT, Jr., Schubert US. Soft Matter 2011; 7: 1581-1588.

[20] Botet R, Roger K. Curr Opin Colloid Interface Sci 2016; 22: 108-112.

[21] Aschenbrenner E, Bley K, Koynov K, Makowski M, Kappl M, Landfester K, Weiss CK. Langmuir 2013; 29: 8845-8855.

[22] Geissler A, Biesalski M, Heinze T, Zhang K. J Mater Chem A 2014; 2: 1107-1116.

[23] Saad WS, Prud'homme RK. Nano Today 2016; 11: 212-227.

[24] Johnson BK, Prud'homme RK. AIChE J 2003; 49: 2264-2282.

[25] Ding S, Anton N, Vandamme TF, Serra CA. Expert Opin Drug Delivery 2016; 13: 1447-1460.

[26] Liu Y, Yang G, Zou D, Hui Y, Nigam K, Middelberg APJ, Zhao C-X. Ind Eng Chem Res 2020; 59: 4134-4149.

[27] Solans C, Morales D, Homs M. Curr Opin Colloid Interface Sci 2016; 22: 88-93.

[28] Stainmesse S, Orecchioni AM, Nakache E, Puisieux F, Fessi H. Colloid Polym Sci 1995; 273: 505-511.

[29] Yan X, Alcouffe P, Sudre G, David L, Bernard J, Ganachaud F. Chem Commun 2017; 53: 1401-1404.

[30] Beck-Broichsitter M, Nicolas J, Couvreur P. Nanoscale 2015; 7: 9215-9221.

[31] Hornig S, Heinze T, Becer CR, Schubert US. J Mater Chem 2009; 19: 3838-3840.

[32] Aubry J, Ganachaud F, Addad J-PC, Cabane B. Langmuir 2009; 25: 1970-1979.

[33] Legrand P, Lesieur S, Bochot A, Gref R, Raatjes W, Barratt G, Vauthier C. Int J Pharm 2007; 344: 33-43.

[34] Mei J, Leung NLC, Kwok RTK, Lam JWY, Tang BZ. Chem Rev 2015; 115: 11718-11940.

[35] Li J, Rao J, Pu K. Biomaterials 2018; 155: 217-235.

[36] Zeng Z, Dong C, Zhao P, Liu Z, Liu L, Mao H-Q, Leong KW, Gao X, Chen Y. Adv Healthc Mater 2019; 8: 1801010.

[37] Tarhini M, Benlyamani I, Hamdani S, Agusti G, Fessi H, Greige-Gerges H, Bentaher A, Elaissari A.

Materials 2018; 11: 394.

[38] Bteich J, McManus SA, Ernsting MJ, Mohammed MZ, Prud'homme RK, Sokoll KK. Mol Pharm 2017; 14: 3998-4007.

[39] Heinze T, Hornig S. In Edgar KJ, Heinze T, Buchanan CM (editors), Polysaccharide Materials: Performance by Design, Vol. 1017. American Chemical Society; 2009. Chapter 9.

[40] Discher BM, Won Y-Y, Ege DS, Lee JC-M, Bates FS, Discher DE, Hammer DA. Science 1999; 284: 1143-1146.

[41] Brinkhuis RP, Rutjes FPJT, van Hest JCM. Polym Chem 2011; 2: 1449-1462.

[42] Zhu H, Xie C, Chen P, Pu K. Curr Med Chem 2019; 26: 1389-1405.

[43] Ma C, Ling Q, Xu S, Zhu H, Zhang G, Zhou X, Chi Z, Liu S, Zhang Y, Xu J. Macromol Biosci 2014; 14: 235-243.

[44] Vu KB, Phung TK, Tran TTT, Mugemana C, Giang HN, Nhi TLP. J Ind Eng Chem 2021; 97: 307-315.

[45] Hu X, Zhang Z, Lu Y, Liu R, Sun L, Parkin IP, Zhang X. Appl Organomet Chem 2019; 33: e4713.

[46] Wang J, Kuang M, Duan H, Chen D, Jiang M. Eur Phys J E 2004; 15: 211-215.

[47] Shin JJ, Kim EJ, Ku KH, Lee YJ, Hawker CJ, Kim BJ. ACS Macro Lett 2020; 9: 306-317.

[48] Wong CK, Qiang X, Müller AHE, Gröschel AH. Prog Polym Sci 2020; 102: 101211.

[49] Higuchi T, Motoyoshi K, Sugimori H, Jinnai H, Yabu H, Shimomura M. Soft Matter 2012; 8: 3791-3797.

[50] Higuchi T, Yabu H, Shimomura M. Colloids Surf A Physicochem Eng Asp 2006; 284-285: 250-253.

[51] Yabu H, Higuchi T, Ijiro K, Shimomura M. Chaos 2005; 15: 047505.

[52] Yabu H, Higuchi T, Shimomura M. Adv Mater 2005; 17: 2062-2065.

[53] Higuchi T, Tajima A, Motoyoshi K, Yabu H, Shimomura M. Angew Chem Int Ed 2008; 47: 8044-8046.

[54] Higuchi T, Tajima A, Yabu H, Shimomura M. Soft Matter 2008; 4: 1302-1305.

[55] Higuchi T, Motoyoshi K, Sugimori H, Jinnai H, Yabu H, Shimomura M. Macromol Rapid Commun

2010; 31: 1773-1778.

[56] Higuchi T, Shimomura M, Yabu H. Macromolecules 2013; 46: 4064-4068.

[57] Varadharajan D, Turgut H, Lahann J, Yabu H, Delaittre G. Adv Funct Mater 2018; 28: 1800846.

[58] Qin S, Li H, Yuan WZ, Zhang Y. Soft Matter 2012; 8: 2471-2476.

[59] Grundy LS, Lee VE, Li N, Sosa C, Mulhearn WD, Liu R, Register RA, Nikoubashman A, Prud'homme RK, Panagiotopoulos AZ, Priestley RD. ACS Nano 2018; 12: 4660-4668.

[60] Xie H, She Z-G, Wang S, Sharma G, Smith JW. Langmuir 2012; 28: 4459-4463.

[61] Yabu H, Motoyoshi K, Higuchi T, Shimomura M. Phys Chem Chem Phys 2010; 12: 11944-11947.

[62] Sosa C, Liu R, Tang C, Qu F, Niu S, Bazant MZ, Prud'homme RK, Priestley RD. Macromolecules 2016; 49: 3580-3585.

[63] Sosa C, Lee VE, Grundy LS, Burroughs MJ, Liu R, Prud'homme RK, Priestley RD. Langmuir 2017; 33: 5835-5842.

[64] Lee VE, Sosa C, Liu R, Prud'homme RK, Priestley RD. Langmuir 2017; 33: 3444-3449.

[65] Li N, Panagiotopoulos AZ, Nikoubashman A. Langmuir 2017; 33: 6021-6028.

[66] Li N, Nikoubashman A, Panagiotopoulos AZ. Soft Matter 2017; 13: 8433-8441.

[67] Li N, Nikoubashman A, Panagiotopoulos AZ. Langmuir 2019; 35: 3780-3789.

[68] Morozova TI, Lee VE, Bizmark N, Datta SS, Prud'homme RK, Nikoubashman A, Priestley RD. ACS Cent Sci 2020; 6: 166-173.

[69] Chambon S, Schatz C, Sébire V, Pavageau B, Wantz G, Hirsch L. Mater Horiz 2014; 1: 431-438.

[70] Liu D, Zhang H, Cito S, Fan J, Mäkilä E, Salonen J, Hirvonen J, Sikanen TM, Weitz DA, Santos HA. Nano Lett 2017; 17: 606-614.

[71] Tajima A, Higuchi T, Yabu H, Shimomura M. Colloids Surf A Physicochem Eng Asp 2008; 313-314: 332-334.

[72] Yabu H, Koike K, Motoyoshi K, Higuchi T, Shimomura M. Macromol Rapid Commun 2010; 31: 1267-1271.

[73] Liu Y, Yang G, Baby T, Tengjisi, Chen D, Weitz DA, Zhao C-X. Angew Chem Int Ed 2020; 59: 4720-4728.

[74] Kong L, Chen R, Wang X, Zhao C-X, Chen Q, Hai M, Chen D, Yang Z, Weitz DA. Lab Chip 2019; 19: 2089-2095.

[75] Li W, Chen Q, Baby T, Jin S, Liu Y, Yang G, Zhao C-X. Chem Eng Sci 2021; 235: 116468.

[76] Baby T, Liu Y, Yang G, Chen D, Zhao C-X. J Colloid Interf Sci 2021; 594: 474-484.

[77] Yan X, Delgado M, Fu A, Alcouffe P, Gouin SG, Fleury E, Katz JL, Ganachaud F, Bernard J. Angew Chem Int Ed 2014; 53: 6910-6913.

[78] Yan X, Sivignon A, Alcouffe P, Burdin B, Favre-Bonte S, Bilyy R, Barnich N, Fleury E, Ganachaud F, Bernard J. Chem Commun 2015; 51: 13193-13196.

[79] Yan X, Ramos R, Hoibian E, Soulage C, Alcouffe P, Ganachaud F, Bernard J. ACS Macro Lett 2017; 6: 447-451.

[80] Yan X, Remond M, Zheng Z, Hoibian E, Soulage C, Chambert S, Andraud C, Van der Sanden B, Ganachaud F, Bretonnière Y, Bernard J. ACS Appl Mater Interfaces 2018; 10: 25154-25165.

[81] Yan X, Ramos RANS, Alcouffe P, Munoz LE, Bilyy RO, Ganachaud F, Bernard J. Biomacromolecules 2019; 20: 3915-3923.

[82] Ramos R, Koh K, Gabryelczyk B, Chai L, Kanagavel D, Yan X, Ganachaud F, Miserez A, Bernard J. ACS Macro Lett 2021; 10: 628-634.

[83] Yan X, Alcouffe P, Bernard J, Ganachaud F. Biomacromolecules 2020; 21: 4591-4598.

Table 1. Formation of mono-component polymeric nanoparticles of controlled nanostructures.

Polymers	Solvent	Non-solvent	Mixing	Nanostructures	Size/nm	Ref
methacryloyl bifunctionalized dextran	THF	Water	Batch	dimpled beads		[21]
poly(1,1,2,2-tetraphenylethene)	THF	Water	Batch	dimpled beads	167~204	[43]
polystyrene	THF	Water	Batch	dimpled beads	~250	[44]
P(S-*co*-AA)	THF	Water	Flash	porous	~210	[45]
Carboxyl-terminated polyimide	THF	Water	Batch	dimpled beads	100~600	[46]
Carboxyl-terminated polyimide	THF	Water	Batch	porous	100~200	[46]
PS-*b*-PI	THF	Water	SORP	stacked lamellar; onion-like; hexagonally-packed cylindrical		[52,54,55]
P(S-co-VBC)-b-PI	THF	Water	SORP	stacked lamellar; onion-like; patchy	140-300	[57]
P(S-co-VBA)-b-PI	THF	Water	SORP	stacked lamellar; onion-like	200-3000	[57]
P(S-co-PFS)-b-PI	THF	Water	SORP	onion-like	140-300	[57]
PtBA-*b*-PFNEMA	THF	Water	Batch	stacked lamellar; onion-like; bicontinuous	310-533	[58]
PS-*b*-PI	THF	Water	Flash	lamellar	30-300 (ordered), 200-700 (disordered)	[59]

Table 2. Formation of multi-component polymeric nanoparticles of controlled nanostructures.

Components	Solvent	Non-solvent	Mixing	Nanostructure	Size/nm	Ref

PLGA	DMSO/THF	Water	Microfluidic	Janus	300	[60]
PS, PI	THF	Water	SORP	Janus		[54]
PS, PI, PS-*b*-PI	THF	Water	SORP	Janus, patchy		[54]
PI-*b*-P2VP, PS-*b*-PI	THF	Water	SORP	Janus;onion-like; packed cylindrical		[61]
PS-*b*-P2VP, PS-*b*-PI	THF	Water	SORP	onion-like; packed cylindrical		[61]
P(S-co-VBC)-*b*-PI, PS-*b*-PI	THF	Water	SORP	stacked lamellar		[57]
P(S-co-VBA)-*b*-PI, PS-*b*-PI	THF	Water	SORP	stacked lamellar		[57]
P(S-co-PFS)-*b*-PI, PS-*b*-PI	THF	Water	SORP	stacked lamellar		[57]
PS, PI	THF	Water	Flash	Janus, patchy	125-540	[62-64]
PS, PS-*b*-PI	THF	Water	Flash	Janus, patchy		[59]
PS, PB	THF	Water	Flash	Janus		[62]
PS, PLA	THF	Water	Flash	Janus		[62]
PLA, PB	THF	Water	Flash	Janus		[62]
PS, PI, PS-*b*-PEG	THF	Water	Flash	Janus	50-660	[68]
PS, PB, polyvinylcyclohexane	THF	Water	Flash	Cerberus		[62]
P3HT@PCBM	THF	DMSO/Water	Batch	Core@shell	77-85	[69]
Paclitaxel@hypromellose acetate succinate	Acetone	Water	Microfluidic	Core@shell	40-450	[70]
Sorafenib@hypromellose acetate succinate	Acetone	Water	Microfluidic	Core@shell	70-550	[70]
PLGA@hypromellose acetate succinate	Acetone	Water	Microfluidic	Core@shell		[70]
PI@PMMA	THF	Water	SORP	Core@shell	273-372	[71]
PIB@PI	THF	Water	SORP	Core@shell		[72]
PS@PMMA	THF	Water	SORP	Core@shell		[72]

PI@PS-NH_2	THF	Water	Flash	Core@shell		[64]
Curcumin@Shellac	DMSO/DMF/EtOH	PBS buffer	Batch	Core@shell	50	[73]
Curcumin@PLGA-b-PEG	DMSO/DMF/EtOH	PBS buffer	Batch	Core@shell		[73]
Curcumin@Shellac and PLGA-b-PEG	DMSO/DMF/EtOH	PBS buffer	Batch	Core@shell		[73]
Paclitaxel@Shellac	DMSO/DMF/EtOH	PBS buffer	Batch	Core@shell		[73]
Paclitaxel@PLGA-b-PEG	DMSO/DMF/EtOH	PBS buffer	Batch	Core@shell		[73]
Paclitaxel@Shellac and PLGA-b-PEG	DMSO/DMF/EtOH	PBS buffer	Batch	Core@shell	100	[73]
Ibuprofen@Shellac	DMSO/DMF/EtOH	PBS buffer	Batch	Core@shell		[73]
Docetaxel@Shellac and PLGA-b-PEG	DMSO/DMF/EtOH	PBS buffer	Batch	Core@shell		[73]
Amphotericin B@PLGA-b-PEG	DMSO/DMF/EtOH	PBS buffer	Batch	Core@shell		[73]
Curcumin@Shellac	DMSO/DMF/EtOH	Water	Microfluidic	Core@shell	86-142	[76]
Hexadecane@PHMM	Water	Actone	Batch	Core@shell	150-250	[77]
Miglyol or Hexadecane@Poly(HMM-stat-GMA)	Water	Acetone	Batch	Core@shell	110 (Miglyol) 118 (HD)	[78]
Miglyol or Hexadecane@PEMM	Water	Acetone	Batch	Core@shell	40-200	[29]
Hexadecane@PHPMA	Water	Acetone	Batch	Core@shell	196-226	[79]
Hexadecane@P(HPMA-*co*-EMM)	Water	Acetone	Batch	Core@shell	91-351	[79]
Hexadecane@P(HPMA-*co*-DEMA)	Water	Acetone	Batch	Core@shell	198-218	[79]
Hexadecane@P(HPMA-co-EMM-co-DEMA)	Water	Acetone	Batch	Core@shell	90, 218, 320	[79]
Miglyol@Dextran	Water	Acetone	Batch	Core@shell	74-220	[81]
Miglyol@Pullulan	Water	Acetone	Batch	Core@shell	386	[81]
Miglyol@Glycogen	Water	Acetone	Batch	Core@shell	150-229	[81]

Miglyol@Dextran Sulfate	Water	Acetone	Batch	Core@shell	152-183	[81]
Miglyol@Hyaluronic acid	Water	Acetone	Batch	Core@shell	187-213	[81]
Miglyol@Dextran and Pullulan	Water	Acetone	Batch	Core@shell	270	[81]
Miglyol@Dextran and Hyaluronic acid	Water	Acetone	Batch	Core@shell	100	[81]
Miglyol@Dextran and Dextran Sulfate	Water	Acetone	Batch	Core@shell	90	[81]
Miglyol@Glycogen and Hyaluronic acid	Water	Acetone	Batch	Core@shell	98	[81]
Miglyol@Dextran/Pullulan	Water	Acetone	Batch	Core@shell	226	[81]
Miglyol@Glycogen and Hyaluronic acid/Dextran/Pullulan	Water	Acetone	Batch	Core@shell	96	[81]
Miglyol@Suckerin-Silk Fusion Protein	Water	Acetone	Batch	Core@shell	200-300	[82]
Hexadecane@Suckerin-Silk Fusion Protein	Water	Acetone	Batch	Core@shell	225	[82]
Miglyol@Dextran and Poly(HMM-stat-GMA)	Water	Acetone	Batch	Core@shell	139-178	[83]
Miglyol@Pullulan and Poly(HMM-stat-GMA)	Water	Acetone	Batch	Core@shell	171	[83]
Miglyol@Dextran, Pullulan and Poly(HMM-stat-GMA)	Water	Acetone	Batch	Core@shell	178	[83]
Miglyol@FITC-Dextran, Biotin-Dextran and Poly(HMM-stat-GMA)	Water	Acetone	Batch	Core@shell	166	[83]
Miglyol@Dextran/Poly(HMM-stat-GMA)	Water	Acetone	Batch	Core@shell	132	[83]
Miglyol@Pullulan/Poly(HMM-stat-GMA)/Dextran	Water	Acetone	Batch	Core@shell	172	[83]

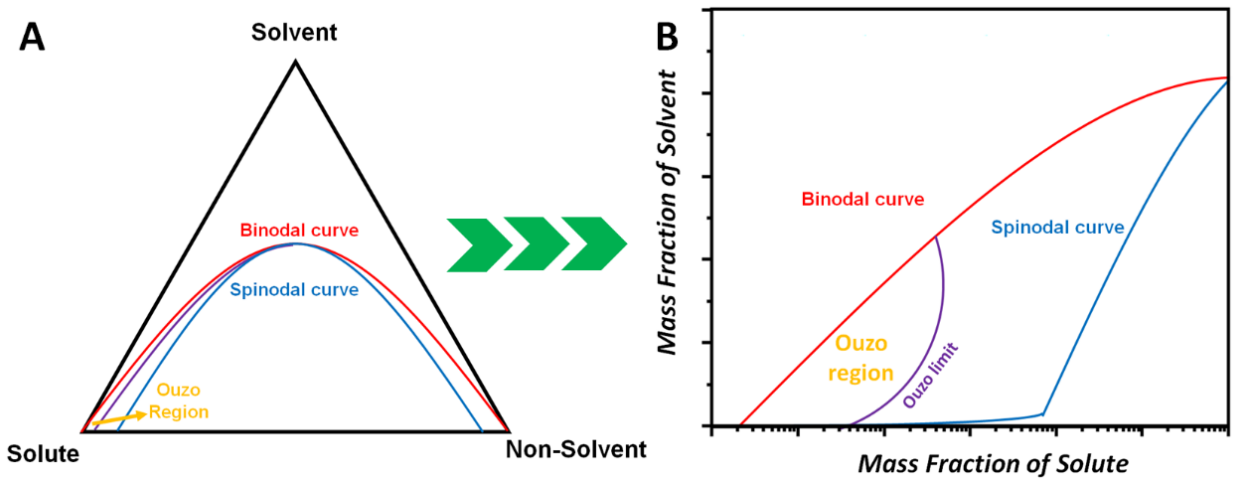

Figure 1. (**A**) Typical triangle solute/solvent/non-solvent ternary phase diagrams in nanoprecipitation; (**B**) Transformed binary phase diagram revealing the Ouzo domain after log-scaling the X axis.

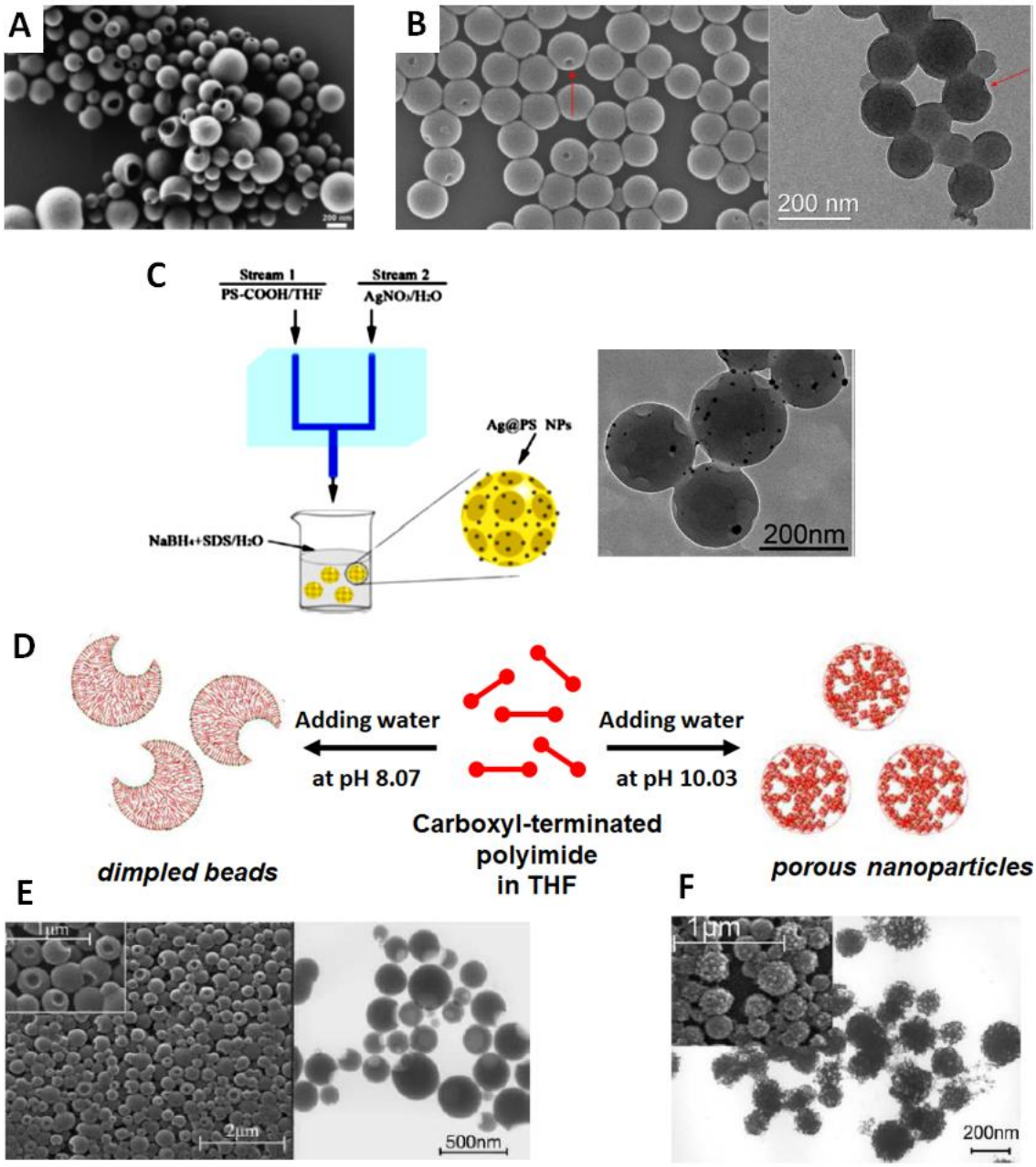

Figure 2. (A) TEM photo of dextran derivatives based nanospheres with a cavity;[21] (B) Scanning electron microscopy (SEM) and TEM images of poly(1,1,2,2-tetraphenylethene) based porous nanoparticles;[43] (C) Schematic illustration of preparation of Ag-loaded PS-based porous nanospheres and TEM photo of nanoparticles;[44] (D) Schematic illustration of preparing carboxyl-terminated polyimide-based porous nanoparticles at different pHs;[45] (E) TEM and SEM photos of carboxyl-terminated polyimide-based dimpled beads with one pore (obtained at pH 8);[45] (F) TEM and SEM images of carboxyl terminated polyimide based porous nanospheres with multiple pores (prepared at pH 10).[45]

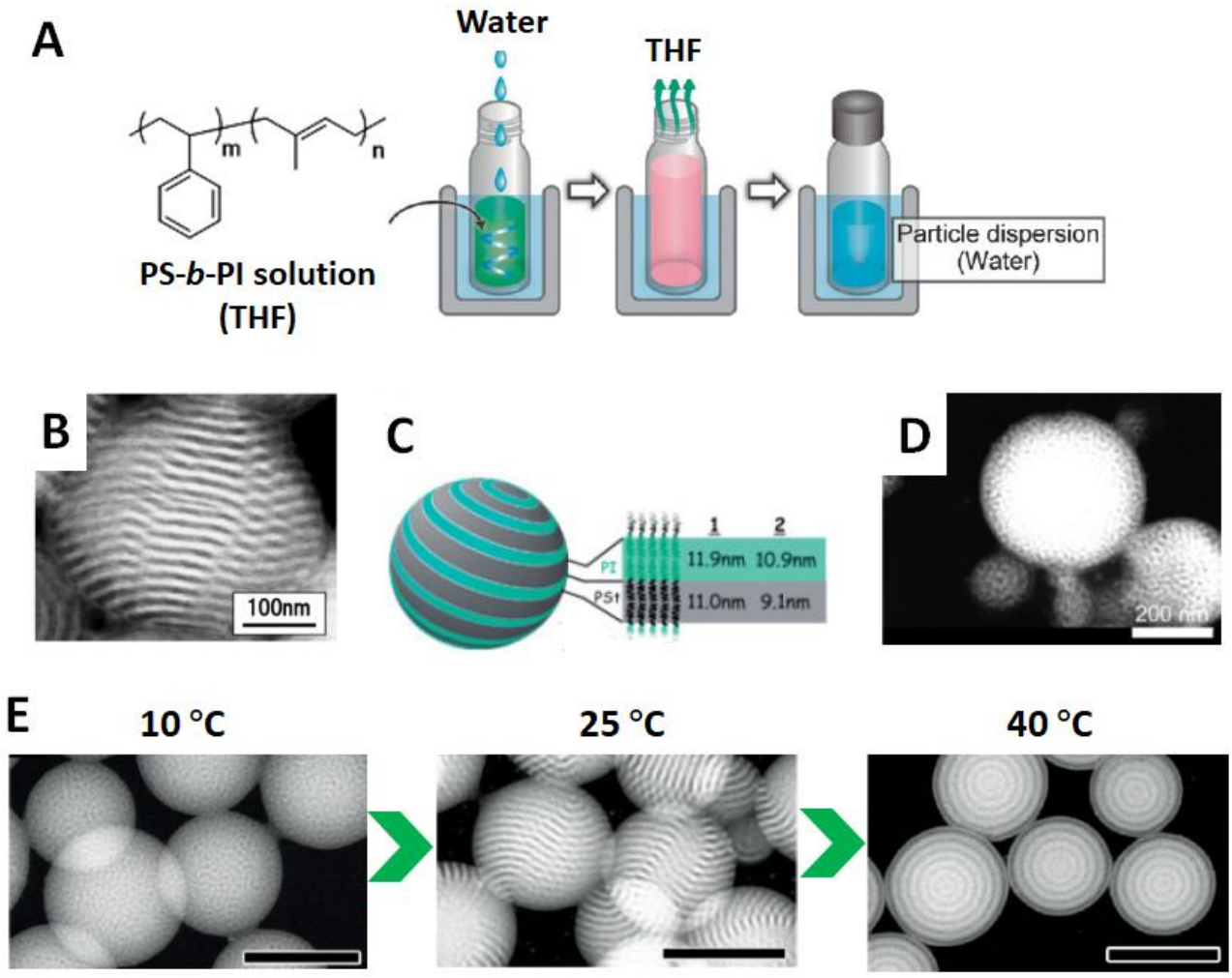

Figure 3. (**A**) Schematic illustration of SORP;[51] (**B**) Scanning transmission electron microscopy (STEM) photo of PS-*b*-PI based stacked lamellar nanoparticles;[51] (**C**) Model of the phase separation of stacked lamellar nanoparticles;[51] (**D**) STEM image of PS-*b*-PI based nanoparticles generated by batch nanoprecipitation;[51] (**E**) STEM images of temperature-controlled morphologies transition in the PS-*b*-PI based nanoparticles, ranging from disordered to stacked lamellar to onion-like structures. Scale bar is 300 nm.[54] PI was stained with OsO_4.

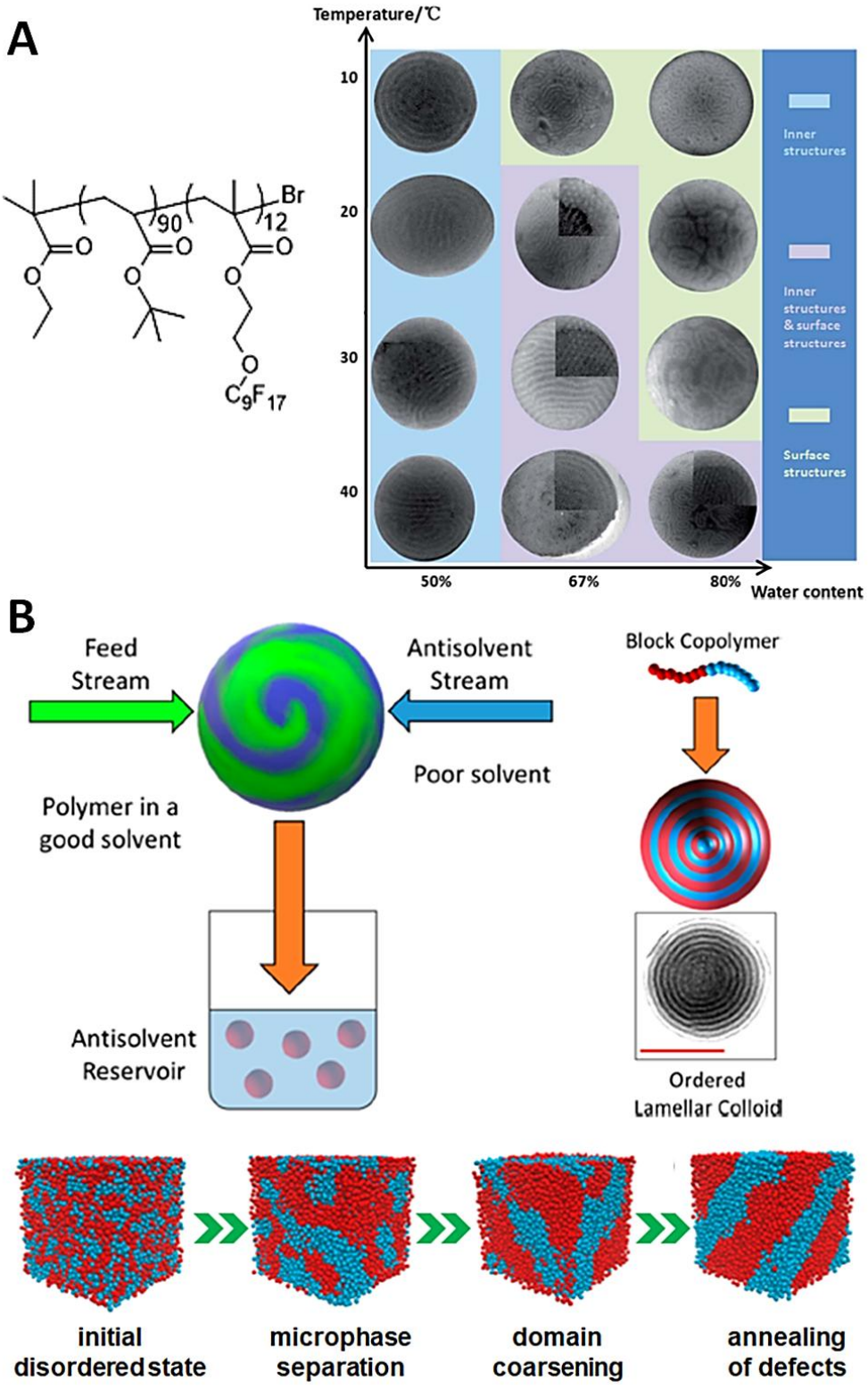

Figure 4. (**A**) Schematic representation of structure transitions of the PtBA-*b*-PFNEMA particles by nanoprecipitation.[57] (**B**) (Top) Schematic illustration of flash nanoprecipitation of PS-*b*-PI block copolymers into ordered lamellar colloids (The particles in TEM image are stained by OsO_4, scale bar is 200 nm), and (Bottom) illustration of the different stages in bulk phase separation of the copolymers according to MD simulation. [58]

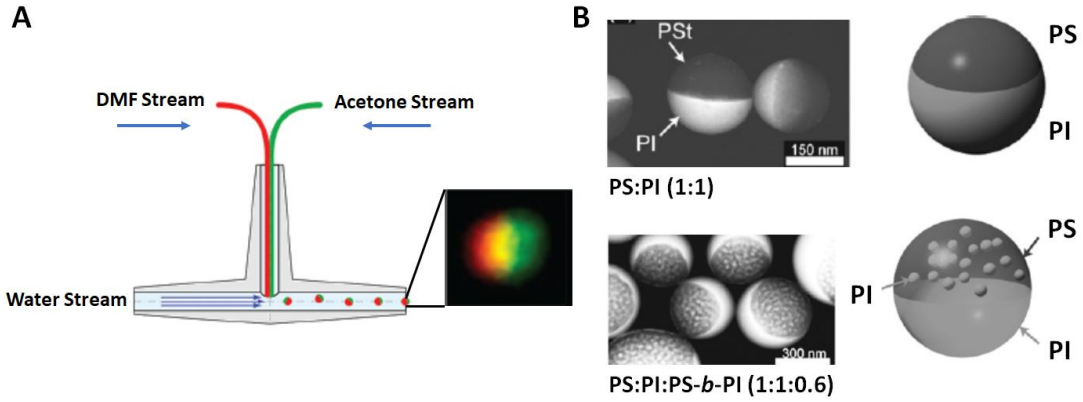

Figure 5. (**A**) Schematic illustration of preparation of PLGA Janus nanoparticles through fluidic nanoprecipitation;[59] (**B**) STEM Images and models of PS-PI and PS-PI-PS-*b*-PI Janus nanoparticles prepared by SORP.[53] PI was stained with OsO_4.

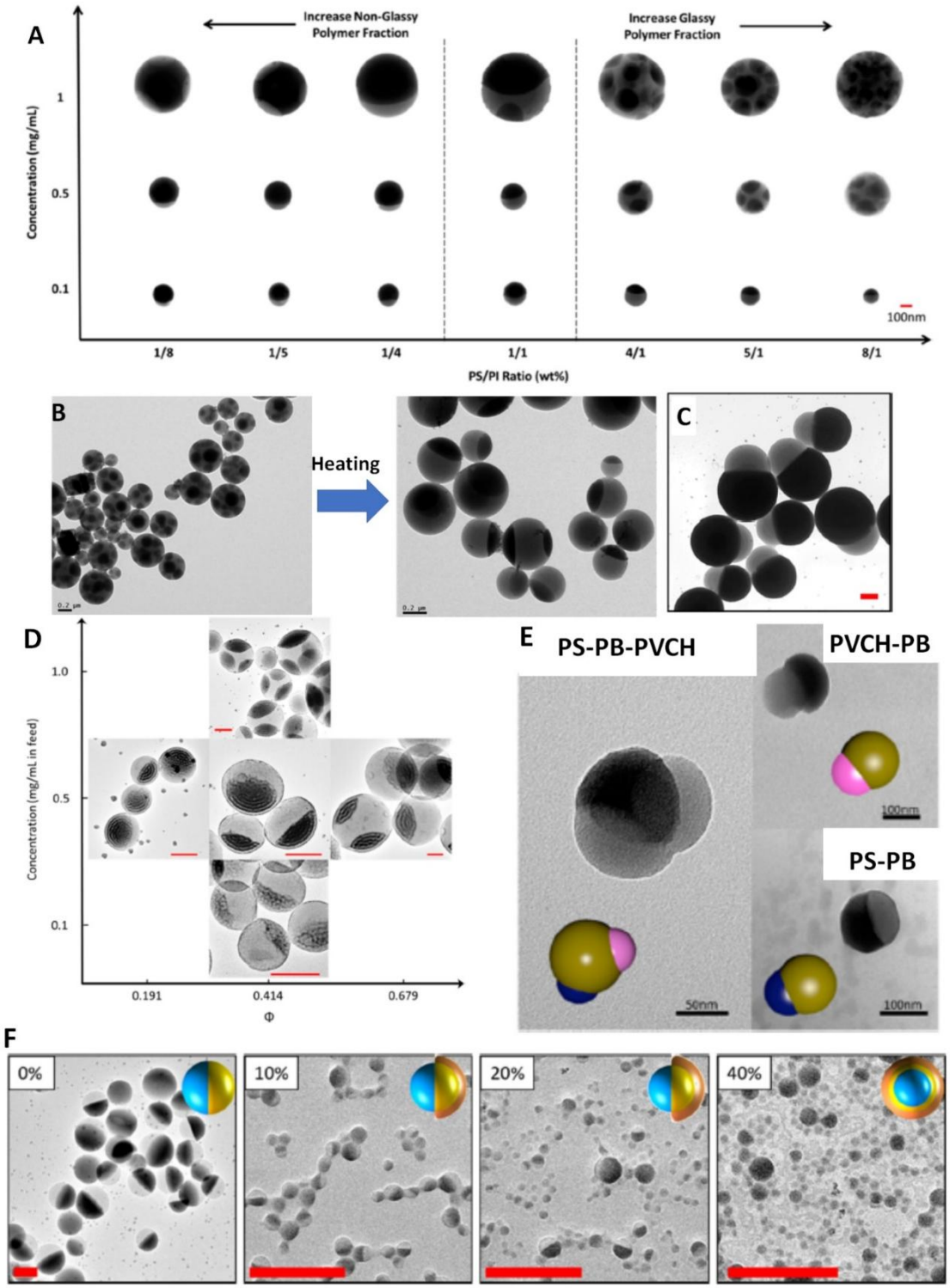

Figure 6. (**A**) Diagram of multi-faceted nanoparticles in various conditions;[62] (**B**) Heating induced morphology transition of multi-faceted nanoparticles;[62] (**C**) TEM images of PS-PI snowman particles, scale bar was 200 nm.[63] (**D**) Blends of PS and PS-*b*-PI at different concentration and volume fraction of homopolymer PS (Φ), scale bar is 200 nm.[58] (**E**) TEM images of PVCH-PB, PS-PB Janus and PS-PB-PVCH Cerberus PNPs.[61] (**F**) TEM images of PNPs prepared from PS-PI mixtures with 0-40 wt% of PS-*b*-PEG, scale bar is 200 nm. PI was stained with OsO_4.

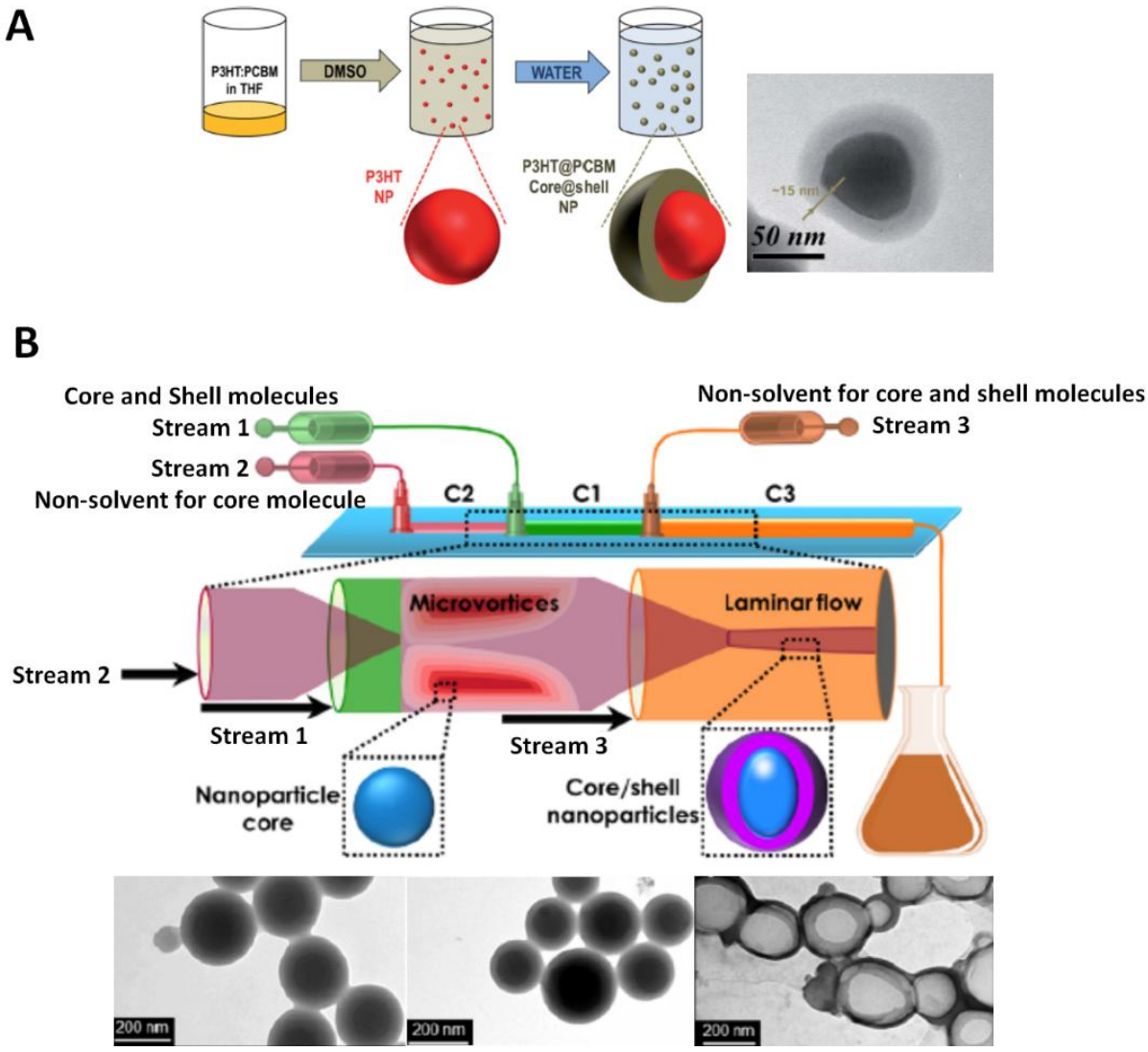

Figure 7. (**A**) Schematic illustration of preparation of semiconducting core/shell NPs through successive batch nanoprecipitation and TEM image of NPs;[68] (**B**) Schematic illustration of core/shell NPs preparation of sequential microfluidic nanoprecipitation and TEM images of paclitaxel@hypro-mellose acetate succinate, sorafenib@hypromellose acetate succinate and PLGA@hypromellose acetate succinate NPs (left to right).[69]

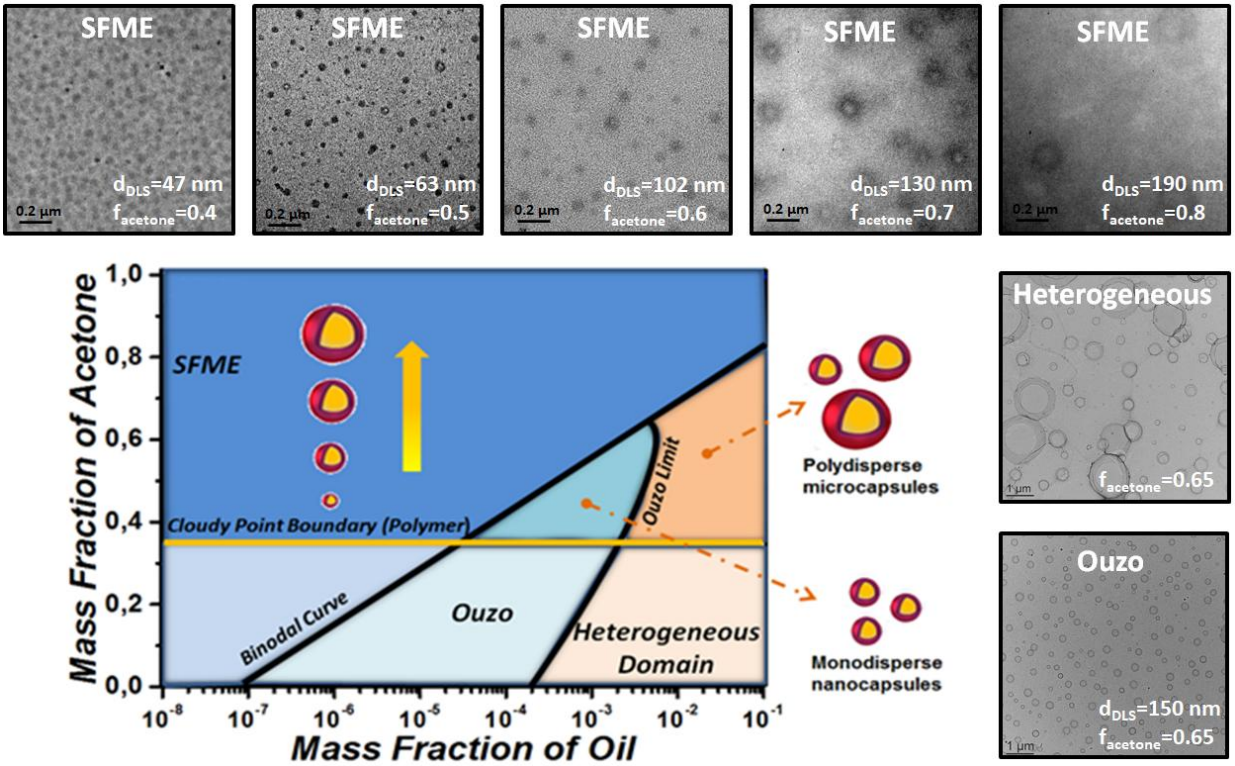

Figure 8. General scheme of hydrophobic oil/hydrophilic polymer/solvent/non-solvent phase diagrams. X-axis presents mass fraction of oil or polymer, Y-axis presents mass fraction of organic solvent. The content of water is deduced from the two others. TEM images of nanocapsules prepared by batch nanoprecipitation of PEMM (in SFME domain)[29] and PHMM (Ouzo and Heterogeneous domain)[72].

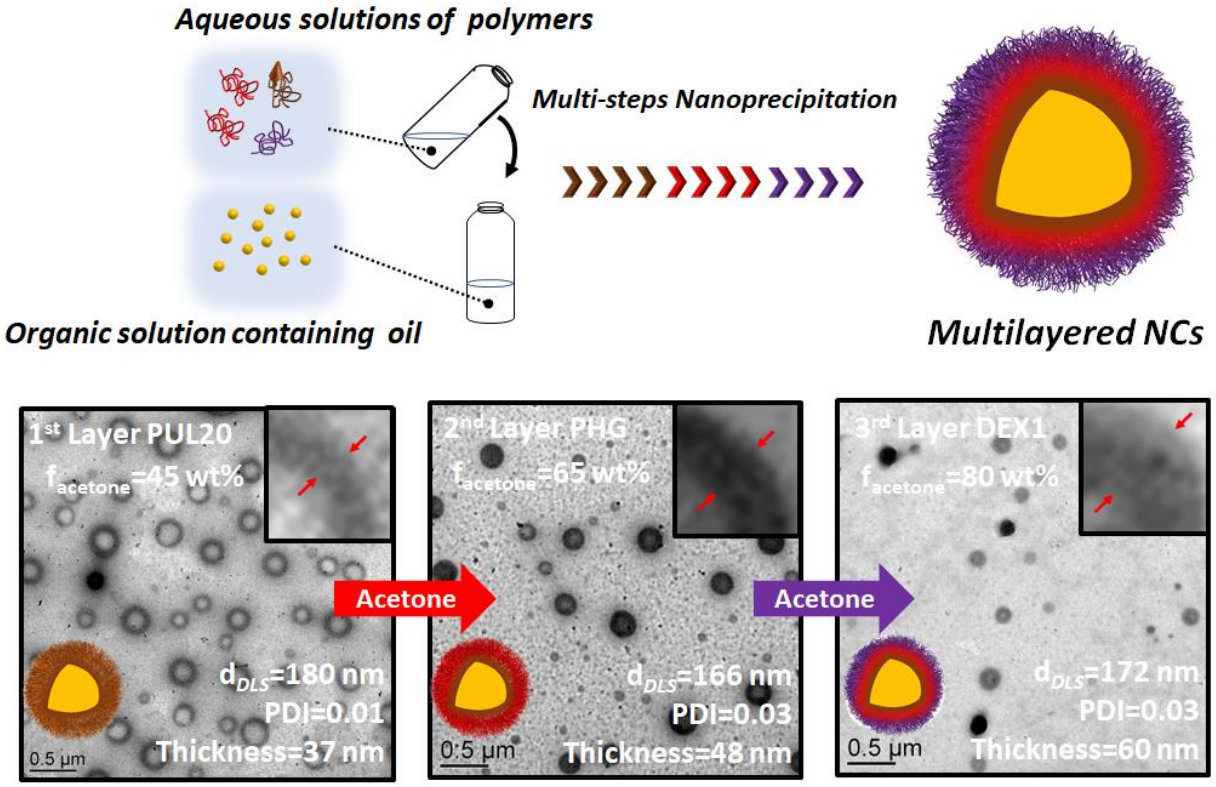

Figure 9. (Top) Schematic illustration of preparation of multilayered polymeric nanocapsules through multi-steps nanoprecipitation.[77] (Bottom) TEM images of trilayered nanocapsules (polymer shell from interior layer to external layer is made of pullulan, PHG (PHMM based glycopolymers) and dextran), inset: zoomed images (10X) of polymeric shell.

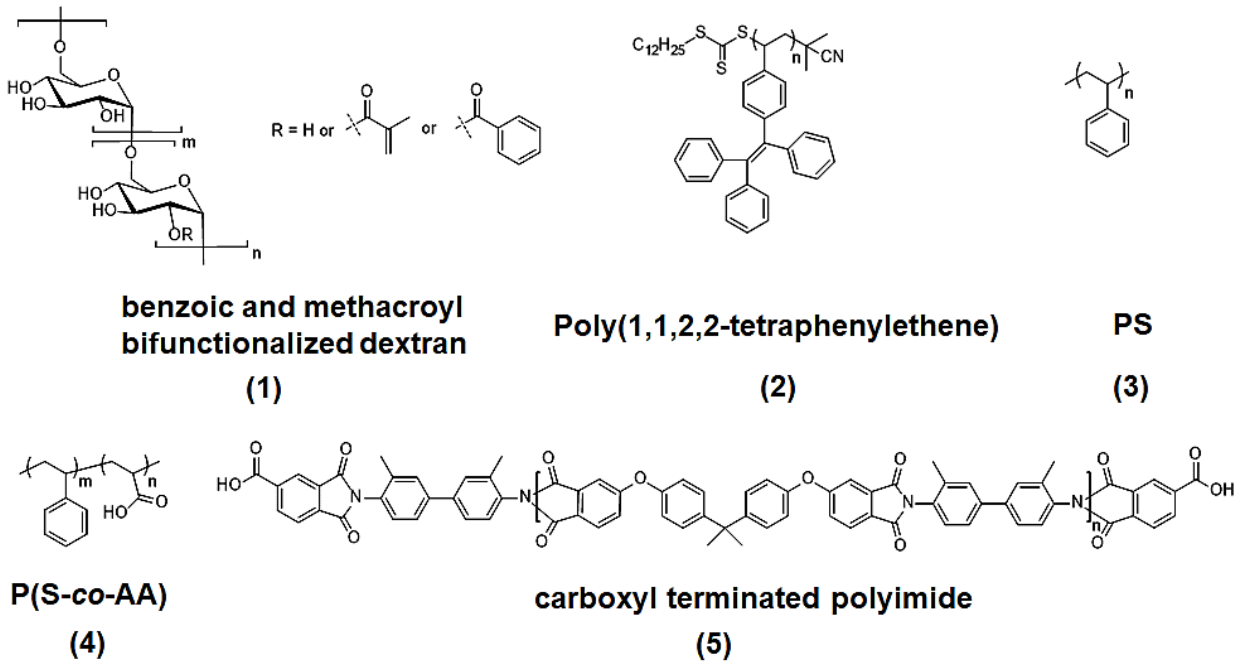

Chart 1. Structures of polymers used to produce porous PNPs by nanoprecipitation.

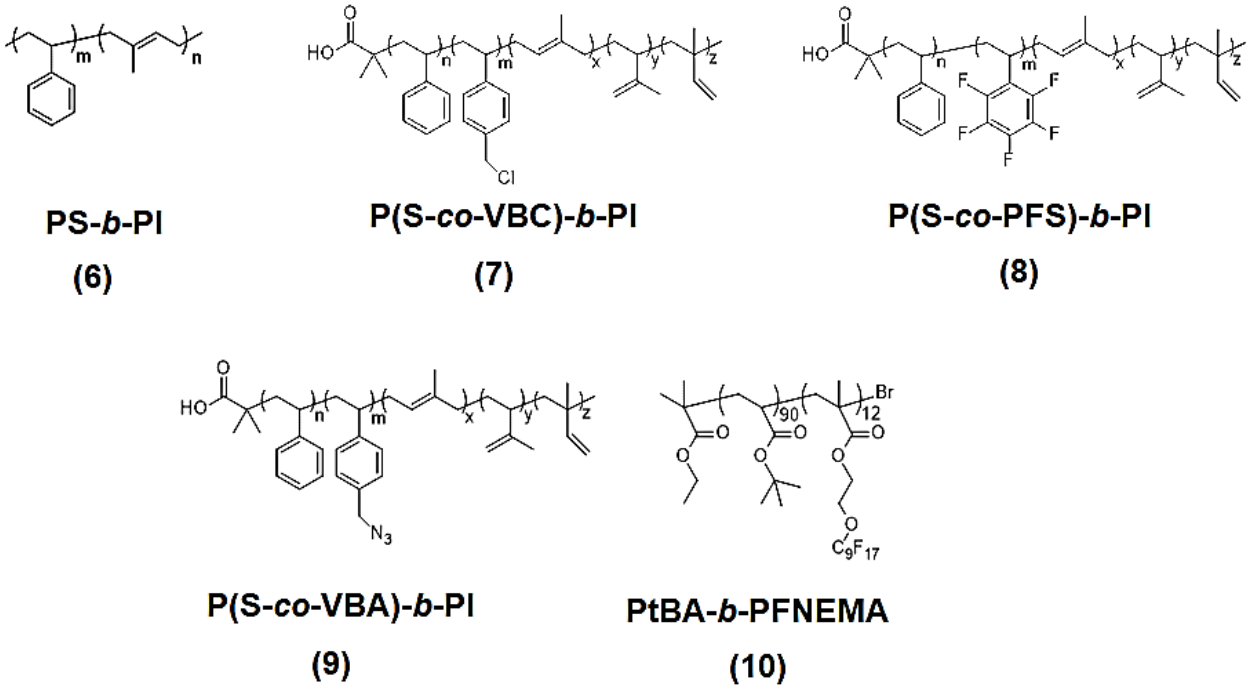

Chart 2. Structures of polymer used to produce complex internally nanostructured PNPs by nanoprecipitation.

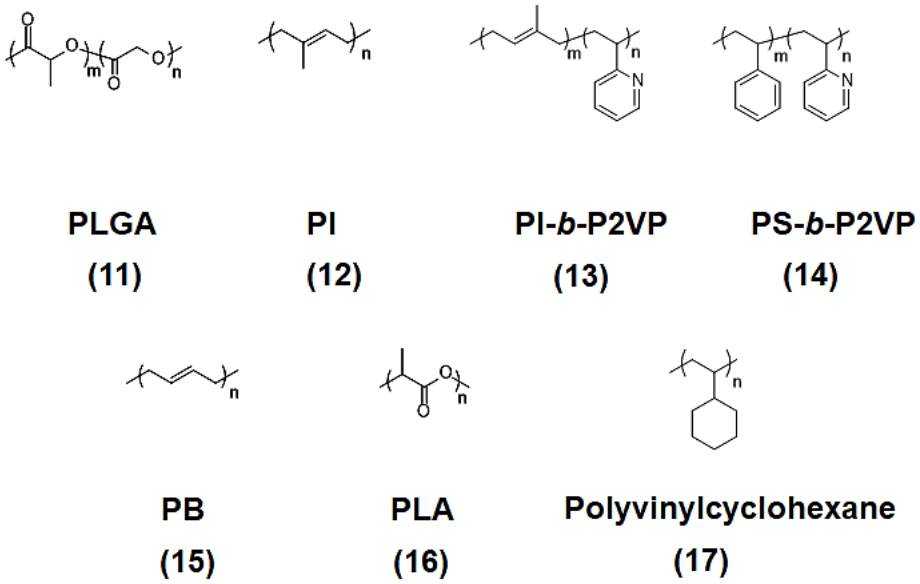

Chart 3. Structures of polymers used to produce multi-faceted PNPs by nanoprecipitation.

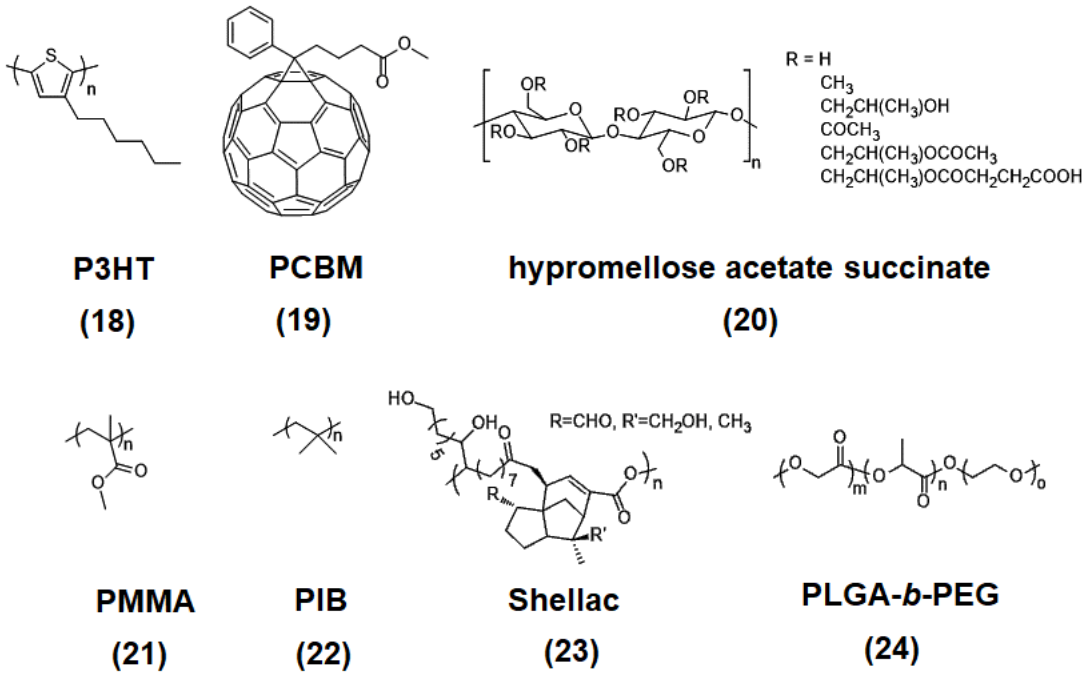

Chart 4. Structures of polymers and functional fullerene used to generate solid-core PNPs by nanoprecipitation.

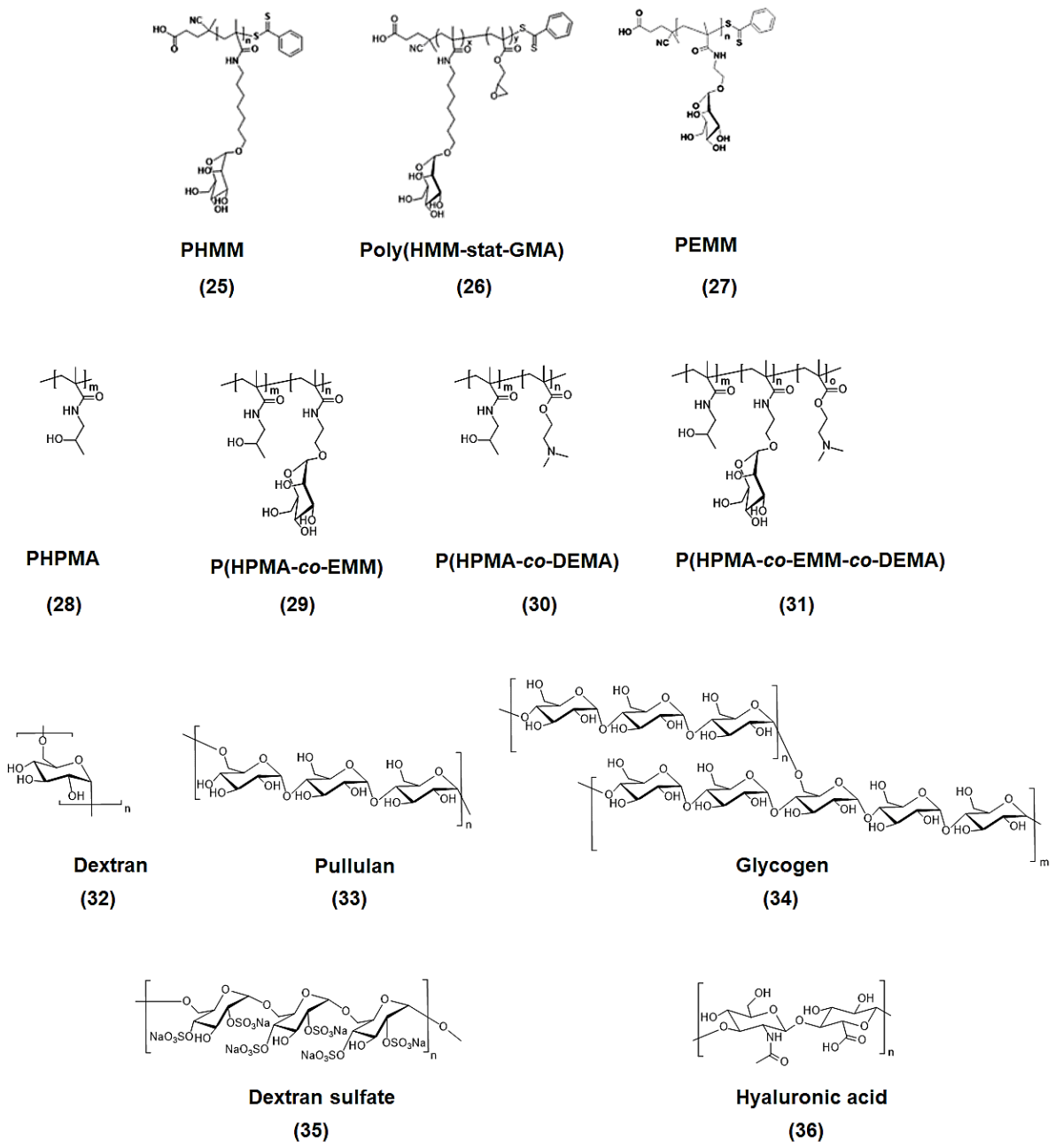

Chart 5. Structures of polymers used to generate oil-core NCs by nanoprecipitation.